NACA RM E51K07

RESEARCH MEMORANDUM

EXPERIMENTAL STUDY OF ISOTHERMAL WAKE-FLOW CHARACTERISTICS OF VARIOUS FLAME-HOLDER SHAPES

By George G. Younger, David S. Gabriel
and William R. Mickelsen

Lewis Flight Propulsion Laboratory
Cleveland, Ohio

NATIONAL ADVISORY COMMITTEE
FOR AERONAUTICS

WASHINGTON

January 23, 1952

NATIONAL ADVISORY COMMITTEE FOR AERONAUTICS

RESEARCH MEMORANDUM

EXPERIMENTAL STUDY OF ISOTHERMAL WAKE-FLOW CHARACTERISTICS OF VARIOUS FLAME-HOLDER SHAPES

By George G. Younger, David S. Gabriel
and William R. Mickelsen

SUMMARY

An investigation of the isothermal wake-flow characteristics of several flame-holder shapes was carried out in a 4- by 4-inch flow chamber. The effects of flame-holder-shape changes on the characteristics of the Kármán vortices and thus on the recirculation zones to which experimenters have related the combustion process were obtained for several flame holders. The results may furnish a basis of correlation of combustion efficiency and stability for similarly shaped flame holders in combustion studies.

Values of the spacing ratio (ratio of lateral spacing to longitudinal spacing of vortices) obtained for the various shapes approximated the theoretical value of 0.36 given by the Kármán stability analysis. Variations in vortex strength of more than 200 percent and in frequency of more than 60 percent were accomplished by varying flame-holder shape. A maximum increase in the recirculation parameter of 56 percent over that for a conventional V-gutter was also obtained. Varying flame-holder shape and size enables the designer to select many schedules of variations in vortex strength and frequency not obtainable by changing size only and may make it possible to approach theoretical maximum vortex strength for any given frequency.

INTRODUCTION

In the design of afterburner and ram-jet combustion elements, which has been largely trial and error to the present time, two general lines of development have emerged. In designs for low burner-inlet velocities or for which pressure losses are a secondary consideration, the basket-type combustor has been successfully applied, at least for a limited range of operating conditions. The use of gutter-type flame holders of various sizes and shapes predominates in applications requiring high inlet velocities and low pressure drops. However, the low burner-inlet pressures and high burner-inlet velocities encountered during high-altitude operation of a combustor employing a gutter-type flame holder produce low combustion efficiencies and limit the stable fuel-air-ratio operating range. It appears that an approach more fundamental

than the trial-and-error procedures previously used will be required to obtain further refinements in the design of gutter-type flame holders.

The fundamental mechanism of stabilization of flames on gutters has recently been studied by several investigators (references 1 and 2). Although many uncertainties still exist in the theory (reference 2), it has become apparent that flame stabilization by bluff bodies is intimately associated with the recirculation zone immediately downstream of the body.

When a bluff body is placed in a fluid stream, surfaces of discontinuity or vortex sheets originate at the point of separation on either side of the body. In isothermal flow, at least, when the Reynolds number is greater than about 30, these vortex sheets roll up into individual vortices which then pass downstream in two parallel stable rows (a Kármán street). The region directly behind the body is essentially unstable and consists of a recirculation zone induced by the vorticity leaving the body before the rolling up process is complete. The strength of the individual vortices in the Kármán street is necessarily proportional to the strength of the vorticity leaving each side of the body. A study of the stable vortex trail therefore provides a useful measure of conditions existing in the unstable region of interest immediately downstream of the bluff body.

The present isothermal investigation was conducted to examine the effects of geometrical changes in the shape of flame-holding bluff bodies on the characteristics of the Kármán vortex trail which may influence the combustion process. The results may be applicable in correlating the combustion performance of similarly shaped flame holders in order to formulate design rules that will permit rational changes in flame-holder design.

A number of variously shaped bluff bodies were investigated at the NACA Lewis laboratory in a flow chamber equipped for visual studies of the flow streamlines and for hot-wire anemometer measurement of the wake-flow periodic frequencies. The bodies were designed to produce variations in strength of the recirculating eddies previously described (having axes perpendicular to the flow direction) and also to superimpose by means of vortex generators a vortex system having an axis approximately parallel to the normal flow direction. A sufficient number of shapes and combinations were investigated to indicate the trends and the order of magnitude of the flow variations that might be induced. Although these results suggested other model shapes, it was impossible to investigate them in the limited time available. The characteristics of the wake flow are presented for these bodies in terms of strength and frequency of the shed vortices. Typical photographs of the flow streamlines are also shown.

SYMBOLS

The following symbols are used in this report:

A_d	flow area of unblocked flow chamber (sq in.)
A_f	projected blocked area of flame-holder model (sq in.)
a	longitudinal spacing of vortices in single row (ft)
b	projected flame-holder model width (ft)
f	vortex shedding frequency (cps)
H	flow-chamber width (ft)
h	lateral spacing between vortex centers in parallel rows (ft)
K	strength of an individual vortex (ft^2/sec)
p_0	approach air-stream static pressure (in. Hg absolute)
R_B	blockage ratio, $A_d/(A_d-A_f)$
Re	Reynolds number based on body projected width
S	Strouhal number, fb/V
u	velocity of vortex system relative to free stream (ft/sec)
V	air-stream velocity past flame-holder model (ft/sec)
V_0	approach air-stream velocity (ft/sec)
V_3	absolute velocity of vortex system (ft/sec)

ANALYSIS

Description of flow field. - The vortex sheets originating from the separation point on a bluff body are unstable and at least in the isothermal case roll up into concentrated individual vortex filaments. The process of rolling up and formation of the individual vortex filaments occurs in a region of short length downstream of the bluff body. It has been observed by numerous investigators that once established the vortices so formed take up positions in the wake far downstream of the body along two lines approximately parallel to the undisturbed streamlines. The vortex centers are arranged at equal spaces along

the rows, and the centers on one row bisect the spaces between centers on the other row. Superimposed on the vortex flow field is the uniform flow passing the bluff body, and the resulting streamlines in the wake observed from a point at rest with respect to the body exhibit a regular sinuous wave form.

Analysis of flow field. - Some analytical considerations of the wake flow, leading to a partial understanding of the behavior of the vortex trail in isothermal flow have been reported by von Kármán (a translation of the original paper is contained in the appendix of reference 3). Experimental examinations of wake flow behind simple bodies are reported in references 4 and 5.

After analyzing the stability of an arrangement of vortices along parallel lines with staggered centers von Kármán concluded (reference 3) that the system is stable: (1) when

$$\cosh \pi \, h/a = \sqrt{3} \quad \text{or} \quad h/a = 0.36 \tag{1}$$

in the neighborhood of the bluff body; or (2) when

$$\cosh \pi \, h/a = \sqrt{2} \quad \text{or} \quad h/a = 0.283 \tag{2}$$

at a great distance from the body (that is, the theoretical spacing ratio diminishes from 0.36 directly behind the body to a limiting value of 0.283 at a great distance from the body). He further showed that the strength of an individual vortex is given by the relation

$$K = \frac{2ua}{\tanh\left(\frac{\pi h}{a}\right)} \tag{3}$$

The velocity of the vortex system relative to the free stream u, which is opposite in direction and lower in magnitude than the undisturbed free-stream velocity, may be calculated from the following equation:

$$u = V_0 - fa \tag{4}$$

It should be noted that the use of V_0 in this equation is valid only for an unbounded medium. Where a finite blockage of the flow field exists, it is necessary to correct for the blockage by using

$$V = \frac{A_d}{A_d - A_f} V_0 = R_B V_0 \tag{5}$$

in the solution of equation (4).

The Kármán analysis assumes (1) nonviscous flow; (2) wake vortices are ideal vortices (that is, having a point discontinuity at the center); and (3) infinite flow field (no wall effects). None of these assumptions is satisfied in the actual flow. In reference 4, it is observed that vortices in the wake of a flat plate are spread over a considerable area and, in fact, the diameters of the vortex cores are approximately equal to the lateral spacing h. Since the origin of the vortices is in the viscous shear layer near the body, the viscous effects obviously may influence the flow to an appreciable extent. Evidence of the influence of Reynolds number is presented in reference 5 in a study of the wake from a cylinder. The wall effects have been investigated in references 5 and 6.

These investigators have found that for real fluids:

(1) The spacing ratio h/a is greater than 0.283 and actually lies between 0.3 and 0.4.

(2) Reynolds number influences the longitudinal spacing between vortices in a single row a and the lateral spacing between vortex centers in parallel rows h (hereinafter called a spacing and h spacing, respectively) but has no effect on the spacing ratio h/a. Reynolds number also affects vortex strength. The critical Reynolds numbers are, however, from 50 to 200 and no appreciable Reynolds number effects have been observed for values up to about 10^5.

(3) Wall effects on strength and spacing ratio are large only if the ratio of body width to channel width b/H is greater than approximately 1/4. However, values of individual a and h spacings may be slightly affected by wall interference for values of the ratio b/H less than 1/4.

Application of analysis to present investigation. - According to one of the theories advanced to explain the nature of stabilization of flames on gutters (references 1 and 2), during combustion hot gases from the burning boundaries of fuel-air mixture surrounding the wake are recirculated upstream and enter the relatively cool boundaries near the body. These hot gases raise the temperature of the surrounding boundaries to the ignition point and combustion of fresh mixture occurs. A portion of the burned mixture is recirculated and a continuous process of ignition is maintained.

The amount of energy required for continuous ignition is a function of burner operating conditions such as local fuel-air ratio, velocity, pressure, and temperature. The heat energy per unit time supplied by the recirculating flow, on the other hand, is a function of the strength and the frequency of shedding of the wake vortices. The flame thus persists as long as the portion of recirculating hot gases is adequate to

balance the requirements of the surrounding mixture. Therefore, for the present investigations, the wake-flow characteristics are expressed in terms of the strength and the frequency of the wake vortices. For each flame holder investigated, the shedding frequency f was determined by means of a hot-wire anemometer, and the individual a and h spacings were determined from photographs of the flow employing balsa-wood particles as flow tracers or from flow surveys. The vortex system velocity u and the vortex strength K could then be determined by solution of equations (3) and (4).

Nondimensional parameters. - A similarity parameter which can be used to express the results of the wake-flow periodic frequency measurements may be derived from equation (4) as follows:

$$f = \frac{V_0 - u}{a}$$

Multiplying by b/V_0 gives

$$\frac{fb}{V_0} = \frac{b}{a}\left(\frac{V_0 - u}{V_0}\right)$$

For the case of finite blockage,

$$\frac{fb}{V} = \frac{b}{a}\left(\frac{V - u}{V}\right)$$

This parameter is frequently denoted the Strouhal number S. A number of investigators (references 7 to 9) have shown experimentally that S is constant and independent of Re (for the range 10^3 to 10^5), size, and velocity for a given body shape. In addition to generalizing the f measurements for a given body shape, S is indicative of the drag suffered in accomplishing an increase in K. Reference 9 points out the inverse relation between S and the measured drag coefficient for circular cylinders over a range of Re from 10^2 to 10^6. As will be shown subsequently, this inverse relation holds for variously shaped bluff bodies at a fixed Re (that is, as the bluffness increases, S decreases).

Because S is constant for a given body shape (over the range of interest) and a function of the ratios a/b and u/V, it is likely that these ratios are also functions of only the body shape. Experimental evidence of the constancy of a/b and u/V for a given body shape is given in references 3 to 5 and 10. The significance of the ratios a/b and u/V is also of interest. The ratio a/b defines the size of

vortices since h/a is a constant (that is, 0.36) and the h spacing is approximately equal to the diameter of the vortex cores (reference 4). If the velocity u (velocity of the vortex field relative to free stream) is assumed conserved in the wake up to the limits of the bluff body, u (or u/V) may be considered as related to the recirculatory mass flow per unit flow area in the sheltered zone. This is verified by examination of figure 1, which shows the recirculation behind one of the flame-holder models at a V_0 of 50 feet per second. As can be seen later the magnitude of the velocity of the recirculating particles (which is determined by comparing the length of the recirculating particle traces with the length of the free-stream particle traces) is approximately equal to the magnitude of the calculated u.

A second empirical parameter which can be used to express the vortex strength results may be obtained from equations (1), (3), and (4) as follows:

Combining equations (1) and (3) gives $K = C_0 ua$ where C_0 is a constant. Combining the preceding equation with equation (4) results in

$$Kf = C_0 u(V_0 - u)$$

Dividing through by V_0^2 yields

$$\frac{Kf}{V_0^2} = C_0 \left(\frac{u}{V_0} - \frac{u^2}{V_0^2} \right)$$

For the case of finite blockage,

$$\frac{Kf}{V^2} = C_0 \left(\frac{u}{V} - \frac{u^2}{V^2} \right)$$

This parameter will be called the recirculation parameter because of its dependence on the ratio u/V. It also is a variable with body shape only.

APPARATUS

Flow chamber. - The present investigations were conducted in a 4- by 4-inch flow chamber connected to the laboratory combustion air and altitude exhaust facilities. A schematic diagram of the flow chamber and attendant equipment is shown in figure 2. Air entered the

apparatus and passed through a honeycomb composed of 1- by 4.5-inch tubes, then through six 50-mesh wire screens. From the calming chamber the air was accelerated to the flow-chamber inlet by a 20.25:1 contraction ratio nozzle. Velocity surveys have shown that the velocity profile was flat to within 0.25 inch of the walls for the range of approach air-stream velocity reported herein.

A 0.0625- by 15-inch slot was provided along the center of a 1.5-inch-thick wall to allow illumination of a narrow plane inside the flow chamber by means of an electronic flashtube subsequently described.

The wall opposite the illumination slot was equipped with fifteen 1-inch-diameter instrumentation plugs which facilitated introduction of the hot-wire probe at various points along the chamber. The sides of the chamber parallel to the plane of illumination consisted of a glass plate and a steel plate. The steel plate was fitted with a plug to facilitate installation and removal of most of the flame-holder models. Both the plug and the glass plate were drilled to receive 0.125-inch-diameter pins which were soldered to the ends of each model. The models were thus held perpendicular to the illumination plane at a point approximately 6 inches downstream of the chamber inlet and in the center.

Balsa wood particles used as flow tracers were introduced into the setup at the nozzle inlet. A detailed description of the injection system finally adopted and the method of processing the balsa dust are given in appendix A.

Camera. - The camera used was a telescoping, wood, box-type camera equipped with an f/4.5 lens having a 7.50-inch focal length. The camera shutter could be actuated remotely from the control panel. A camera arrangement to give a compromise between size and distortion was used, and image size was about one-half actual size for this arrangement. The camera was focused on the flow field at a point 4 inches downstream of the flame-holder gutter edge for most of the photographs. Pictures were taken using 5- by 7-inch triple S orthochromatic cut film.

Light source. - The light source used for the photographic investigation was a General Electric FT 126 xenon-filled flashtube, and the system was essentially the same as that described in reference 1. The flashtube had a 0.25-inch-diameter straight stem approximately 5 inches long, an over-all length of 9 inches, a maximum loading of 60 watt-seconds, and a maximum output of approximately 2100 lumen-seconds. Maximum loading was used with 2000 volts imposed across the tube. The duration of the flash was approximately 150 microseconds as determined from measurements of particle traces at known stream velocity.

The flashtube was mounted 1.5 inch behind the illumination slot with one end of the stem portion directly opposite the model gutter edge. A circular arc reflector was placed behind the flashtube.

Flame-holder models. - The principal variations in the design of all the flame-holder models investigated are summarized in table I. For the primary investigation, the flame-holder models (1 to 12) were designed in the attempt to change the strength of the vorticity leaving the gutter edge. Two methods were used to accomplish this variation in strength:

(1) The velocity gradients at the gutter edge were changed by either altering the shape of the gutter or through the addition of edge tabs or small airfoil sections.

(2) A second vortex system having axis essentially perpendicular to the shed vortices was superimposed on them by utilizing vortex generators (that is, tip vortices).

All flame-holder models used in the primary investigation (figs. 3(a) to 3(l)) were comprised in part of two-dimensional gutters fabricated from 0.062-inch-thick stainless steel which were 4 inches long and had projected widths of 0.75 inch. All V-gutters had 30° included angles.

The flame holders which were designed to obtain a variation in the velocity gradient by changing the shape of the gutter were (1) a conventional V-gutter (flame holder 1, fig. 3(a)), (2) a cambered V-gutter (flame holder 2, (fig. 3(b)), (3) an extended V-gutter (flame holder 3, fig. 3(c)), and (4) a U-shaped gutter (flame holder 4, fig. 3(d)). In designing these models it was reasoned that cambering would increase the velocity gradient at the edge (that is, vortex strength) over that for the conventional V-gutter, that the extension of the V-gutter would influence the strength by reason of the thicker boundary layer in the region of the gutter edge, and that the U-shaped gutter with the zero angle of attack of the sides would give a correspondingly low velocity gradient and accompanying low vorticity strength.

The flame holders which were designed to accomplish a variation in the velocity gradient through the addition of edge tabs or small airfoil sections were (1) a V-gutter with knife edges placed upstream of the gutter edge (flame holder 5, fig. 3(e)), a V-gutter with knife edges placed even with the gutter edge (flame holder 6, fig. 3(f)), a V-gutter with rounded tabs (flame holder 7, fig. 3(g)), and a V-gutter with small airfoils mounted parallel to the gutter (flame holder 8, fig. 3(h)). The shape of the tabs used in the design of these flame holders was purely arbitrary. In the design of flame holder 8 it was hoped that the vortices shed from the airfoil sections would combine with the vortex sheet initiating at the gutter edge and increase the vortex strength.

The flame holders designed to vary the vortex strength by superimposing a longitudinal vortex field on the transverse shedding vortices consisted of V-gutters on which vortex generators were mounted so that the path of the trailing vortices would fall along the bounding surface of the shed vortices. Vortex generators for these flame-holder models were mounted at a 16° angle of attack with the air stream, had an aspect ratio of 0.50, and, when pairs were used, were arranged to produce counterrotating trailing vortices. These flame holders were: (1) a V-gutter with a pair of 0.25-inch-span airfoil sections mounted on each side (flame holder 9, fig. 3(i)), (2) a V-gutter with a pair of 0.25-inch-span flat plates mounted on each side (flame holder 10, fig. 3(j)), (3) a V-gutter with a single 0.56-inch-span flat plate mounted on each side (flame holder 11, fig. 3(k)), and (4) an extended V-gutter with a single 0.56-inch-span flat plate mounted on each side of the plate upstream of the V-gutter (flame holder 12, fig. 3(l)).

In addition to the flame-holder models used in the primary investigation, two models similar to their counterparts in shape but having different gutter widths were used to determine the effects of blockage and varying projected widths. These models were: (1) a conventional V-gutter having a 1.50-inch projected width (flame holder 1A, fig. 3(m)), and (2) a cambered V-gutter having an 0.88-inch projected width (flame holder 2A, fig. 3(n)). A 0.75-inch-diameter circular cylinder (fig. 3(o)) and a 0.75-inch-wide flat plate (fig. 3(p)) were also used in the investigation to determine the agreement of the measurements with the work of previous investigators who have used these shapes most frequently.

INSTRUMENTATION

Air flow, temperature, and pressure. - Air flow was measured with a calibrated variable orifice. The flow chamber inlet-air temperature and static pressure were measured at the points indicated in figure 2. Air temperature was practically constant at 80° F throughout the investigation.

Hot-wire anemometer. - The hot-wire anemometer equipment used in the investigation was the NACA designed constant-temperature hot-wire anemometer which is described in detail in reference 11. The essential parts of this equipment are the usual Wheatstone bridge circuit, amplifier, and oscilloscope. An audio oscillator was used to obtain a Lissajous figure during the vortex-shedding frequency measurements. The wires used throughout the investigation were 0.0002-inch-diameter, 0.10-inch-long tungsten wires mounted in accordance with a method developed by the National Bureau of Standards; namely, copper plating the ends of the wire and soldering to the prongs. The probe diameter was 0.25 inch.

METHOD AND PROCEDURE

Photographic data. - It was desirable to check the vortex a spacing at two air-flow velocities to verify its independence of velocity, and at a flow-chamber pressure that was typical of altitude operation with an afterburner or ram-jet engine. However, the flow velocity at which photographs could be taken was limited because of the increased deviation of the balsa dust particles from the flow path with increased velocity. The limiting chamber pressure for proper balsa-dust injection was about 20 inches of mercury absolute. Accordingly, a V_0 of 50 feet per second and a p_0 of about 20 inches of mercury absolute were selected after taking a series of trial photographs at various flow conditions. A V_0 of 25 feet per second was chosen arbitrarily as the second velocity setting. The Reynolds numbers (based on b) for these conditions are approximately 12,000 and 6000, respectively, as compared with a Reynolds number of about 32,000 for a typical burner operating at a corresponding pressure.

Prior to each photographic run, checks on the air-flow and pressure settings were made to insure agreement to within ±0.50 inch of mercury of the nominal value of pressure setting and to within ±1 inch of water of the nominal value of air-flow setting. This air-flow discrepancy represents a maximum error of ±8 percent in the flow-chamber velocity (at 25 ft/sec). It should be pointed out, however, that as the air flow varied the flow-chamber pressure tended to vary in a compensatory manner; thus it is expected that the maximum error in the velocity due to air-flow changes is less than ±8 percent.

Velocity surveys. - Velocity-pressure surveys were made across the wakes of several models at a point approximately 4 inches downstream of the flame-holder model edge. A micromanometer was used to measure the pressure deflection. These surveys were used to supplement the photographic data on h spacing and the method of interpreting the profiles is described in appendix B along with the method of data reduction.

Frequency measurements. - For the f measurements, the 0.25-inch-diameter hot-wire probe was mounted in one of the instrumentation plugs located in the center of the wall approximately 2.5 inches downstream of the gutter lip. The wire was mounted transverse to the air stream and adjusted laterally for each model investigation until the strongest signal was indicated on the oscilloscope screen. The oscillator frequency was then adjusted until the hot-wire signal and oscillator signal were in phase as indicated by the Lissajous figure. A calibration of the audio oscillator indicated that the read frequencies were about 8 percent high over the range of frequencies investigated and were adjusted accordingly.

Frequency data were taken at a nominal V_0 of 50, 75, and 100 feet per second and at a nominal p_0 of 20 inches of mercury absolute for each flame-holder model. Flow conditions were tabulated so that the actual velocity could be computed for each run.

RESULTS AND DISCUSSION

The laws governing combustion in the wakes of bluff bodies are still not understood. The process is complicated by the interrelations of the factors involved. Some of the known factors which probably influence the combustion process are the recirculatory mass flow per unit area, thermal quenching factors, the time of transmission of a given parcel of gas in the recirculation zone (all of which are interrelated), and the volume of the undisturbed gas within the flame holder.

It has been previously noted that recirculation is measured in terms of the velocity u in the isothermal case. The time of transmission of the hot gases (that is, the frequency of the vortex shedding for a certain size vortex) together with the quantity of material in transport (recirculatory mass flow) determine the ignition energy supplied to the fuel-air mixture as it passes over the flame-holder gutter edge. Qualities inherent in the flame-holder design, such as the surface area and other heat-transfer characteristics, as well as the properties of the approach gas stream may also influence the quenching properties.

The variation of the recirculation and time factors (the K and f of the wake vortices) with flame-holder design is discussed subsequently. It is not known what relation between K and f would provide optimum conditions for combustion; however, it will be shown that by proper selection of flame-holder shape the relation between K and f and hence the various parameters may be widely varied. Subsequent combustion studies may then establish the desirable relation between K and f.

Comparison of results for circular cylinder and flat plate with results of previous experimenters. - It was considered desirable to check the consistency of the data by making a comparison with results obtained by other experimenters who have studied the wakes of cylinders and flat plates. Such experiments utilized both the hot-wire anemometer technique (reference 4) and the photographic technique with bodies set in motion in still fluids (reference 5).

Data were therefore obtained during the present investigations for a circular cylinder and a flat plate each having b equal to 0.75 inch. The results of the f measurements for the circular cylinder are shown in figure 4. The experimental results (data points) are compared with the empirical values (dotted line) given by the Rayleigh equation (references 7 and 12) for the f for a circular cylinder, namely:

$$f = \frac{0.195\ V_0}{b}\left(1 - \frac{20.1}{Re}\right)$$

The solid line shows the values given by the Rayleigh equation solved using V. The agreement between this line and the experimental values justifies the use of V to correct the f and K computations for the physical blockage of the flow field. However, this correction does not account for the effects of the walls on the geometry of the wake, which will be dealt with in a subsequent section of this report.

The following table presents a comparison of parameters for the cylinder and flat plate with some of the available data:

Source	Circular cylinder			
	a/b	h/b	u/V	fb/V
Experimental	4.2	[a]1.5	0.19	0.19
Reference 5[b]	4.15	1.35	.19	-----
Reference 12	----	----	----	.195

	Flat plate		
	a/b	fb/V	Kf/V^2
Experimental	5.0	0.17	0.3
Reference 4[c]	5.25	.146	.56

[a]Calculated using value of h/a = 0.36.
[b]Extrapolated to Re = 12,000 at b/H = 0.19.
[c]For negligible wall effects.

For the cylinder, the agreement of the results with data from reference 5, where wall effects are taken into account, is good. Considering that the results for the flat plate are compared with data obtained in a flow channel where blockage and wall effects are negligible (reference 4), the agreement is considered adequate.

Wall effects. - There are two chief complications introduced by the proximity of the walls of the flow chamber to the bluff body being studied. These complications are: (1) the effect of the actual physical blockage of the flow field with the attendant increase in air velocity over the bluff body; and (2) the effect on the geometry of the wake due to the interaction between the vortices generated by the body and the walls of the flow chamber. The blockage effect is accounted for by using V in all data computations involving velocity. The wall effect is not so easily taken into account although its effect may be appreciable in some cases.

Reference 5 presents the only available experimental data on wall effects. The effect of increased blockage is to reduce a/b. Data obtained with flame-holder models 1, 1A, 2, and 2A along with data from reference 5 are shown in figure 5 in a plot of a/b against b/H for Reynolds numbers greater than 400. It can be seen that the flame-holder data lie on curves parallel to data from reference 5, indicating the presence of wall effects. The wall effects could be accounted for by extrapolating the curves in figure 5 to $b/H = 0$ (that is, a flow channel of infinite width), which would give a/b equal to a constant for a given shape. However, a separate curve for each flame-holder shape investigated would be required to make a satisfactory adjustment of the data. Because insufficient time was available to obtain these data, experimental values of a spacing were used in the computation of K. In addition, the data presented are for a single value of blockage. Accordingly, and with the assumption that the wall-effect curves would be parallel for the various flame-holder shapes, the K values for this report are subject to the following qualifications:

(1) The magnitudes are slightly higher than those which would be obtained for flame holders in an infinite flow field (that is, K increased with decreasing a for shapes investigated).

(2) They are correct relative to each other since b is the same for all flame-holder models (0.75 in.).

(3) The relative differences are approximately correct because adjusting the data would lower all values by nearly proportionate amounts.

Wake-flow characteristics. - The following table presents a tabulation of the average h/a values computed from photographic data for several flame holders:

Flame holder	2	3	4	5	7	8	12	1A	Cylinder	Flat plate
Average lateral spacing, h, in.	1.03	1.03	0.846	1.08	1.09	0.903	0.910	1.31	1.09	1.30
Spacing ratio, h/a	0.356	0.389	0.347	0.345	0.369	0.357	0.377	0.336	0.358	0.346

The h spacing measurements were obtained from two photographs picked at random for each flame holder. The procedure is explained in detail in appendix B.

It will be noted that the values of h/a approximate the value of 0.36 given by the Kármán stability analysis. This ratio is verified also by using values of h spacing obtained from the wake velocity profiles. Typical velocity profiles for flame holder 8 and the flat plate are shown in figures 6(a) and 6(b), respectively. The values of $h/2$ were obtained for these surveys by determining the inflection point in the curve in accordance with the procedure explained in detail in appendix B. The a spacing used in the computation of the spacing ratio was the average value obtained from the photographic data. Because the spacing ratio obtained by the two methods agreed reasonably well with the value of 0.36 obtained theoretically by Kármán, it was assumed to be 0.36 in all cases. A given percentage variation in the spacing ratio causes a lesser percentage change in K; therefore it is believed that the accuracy of the results is not impaired by using a value of 0.36.

Typical results of the f measurements are shown in figure 7 for flame-holder models 2, 4, 5, and 9. The f and K results are summarized in figure 8 for all flame-holder shapes investigated. Note that f and K are linear functions of V_0 (or V) for any given shape. Figure 8 indicates that f varied, in extremes, over 60 percent and that K varied over 200 percent because of changes in flame-holder shape.

Typical flow visualization photographs at a V_0 of 25 feet per second are presented in figure 9 for flame holders 4, 5, and 6. Figure 10 shows typical flow-visualization photographs at a V_0 of 50 feet per second for flame holders 1, 8, and 11. A tabulation of the measured variables and calculated parameters for all flame-holder models is presented in table II for a V_0 of 50 feet per second.

Effect of flame-holder design on K and f. - The computed variation of K with a spacing (plot of equation (3)) for a V of 62 feet per second (that is, V_0 equal to 50 ft/sec) and an h/a of 0.36 is shown in figure 11 for constant values of f. Experimental results for all flame-holder shapes investigated are shown superimposed on figure 11. It might be desirable to operate near the peaks of the constant frequency curves (dashed line in fig. 11) in order to have maximum K for maximum recirculation. The value of this type of plot, therefore, is to show the position of the experimental points in relation to the maximums and also to point out some of the general trends of varying flame-holder shape on the K-f spectrum.

Several significant results of varying flame-holder shape are apparent in figure 11. A definite trend of increasing K and decreasing f is provided by the flame holders having varying velocity

gradients in the gutter-edge region. In this trend, the U-shaped flame holder (number 4) has the lowest K and the highest f, and the conventional V-gutter (number 1), the extended V-gutter (number 3), the cambered V-gutter (number 2), and the V-gutters with tabs (numbers 5, 6, and 7) are arranged in a corresponding order of increasing K and decreasing f. Evidence which supports this trend is given in reference 10 in which an ogival model, wedge, cylinder, and flat plate are grouped in order of increasing velocity gradients as determined from hot-wire anemometer measurements. The higher relative value of velocity gradient for the flat plate in reference 10 as compared with the relative K value obtained herein is probably due to the fact that the flat plate had a much sharper edge than that used for the present investigations. It is apparent (using the conventional V-gutter as a basis of comparison) that increasing the velocity gradient (cambering, building up the boundary-layer thickness, or increasing the bluffness) increases K and decreasing the velocity gradient (reducing the bluffness) decreases K, substantiating the anticipated results.

No appreciable change in K results from superimposing a secondary vortex system on the shed vortices by means of vortex generators (flame holders 9, 10, 11, and 12). However, a slight increase in K with increased size of vortex generators is indicated (flame holders 11 and 12). Flame holder 12 for which the secondary vortex system intercepts the gutter edge instead of the wake appears to provide the greatest increase in vortex strength. Additional effects on K could probably be obtained by varying size, number, and angle of attack of the vortex generators on these flame holders. Even though the change in K is slight for these flame holders, combustion may still be influenced because of the difference in mixing process downstream.

It should be noted that the results for flame holder 8 are subject to error because the effective b is less than 0.75 inch. A flame holder having the same shape but an effective b of 0.75 inch should have a higher K than flame holder 1.

Lines of constant shape and variable b (these are also lines of constant u/V) are straight lines through the origin intercepting the experimental points. Such a line is shown for the conventional V-gutter (flame holder 1). It is of interest to note that the peaks of the constant frequency curves may not be simply approached by varying width for a given shape; however, indications are that the peaks may be approached by varying shape.

The experimental results are presented in figure 12 in a plot of K/V against f/V. Since K and f are linear functions of V, this plot is independent of V. In general, the trends in this plot are the same as those in figure 11. The lines of varying b in this type of plot are hyperbolic curves passing through each experimental point.

Typical curves (dashed lines) are shown in figure 12 for flame-holder models 1, 4, and 6. The slopes of the variable b lines increase with decreasing f/V (increasing b) for a given shape. The wide choice of K and f combinations available by changing flame-holder shape which cannot be obtained by changing width at constant shape is apparent in figure 12. Note, for example, that flame holder 4 can never have the same K and f as flame holder 1.

A plot of recirculation parameter against S for all flame-holder shapes investigated is presented in figure 13. This plot is independent of both b and V and therefore represents directly the changes in K and f that can be obtained by varying shape instead of size. Figure 13 also indicates the increased drag (as evidenced by the decreased S) that accompanies an increase in K. The theoretical maximum K for any given f (that is, the dashed curve in fig. 11), which is also the maximum value of the recirculation parameter, is a horizontal line through Kf/V^2 equal to 0.615 in figure 13 as shown. This value is obtained by noting that the value of u/V for which K is a maximum for a given f is 0.5.

A maximum increase in the recirculation parameter of 56 percent over that for a conventional V-gutter was obtained by varying shape. A corresponding decrease in S of 21 percent accompanied the change in recirculation parameter. As previously noted, it may be possible to approach the theoretical maximum K for any given f ($Kf/V^2 = 0.615$) by considering other shapes not investigated herein or by modifying the design of the vortex-generator-type flame holders.

CONCLUDING REMARKS

Varying flame-holder shape enables the designer of flame holders to select many schedules of variation of vortex strength and shedding frequency not obtainable by changing size with a given shape. Indications are that it may be possible to approach theoretical maximum vortex strength for any given frequency by varying shape as well as size. Variations in vortex strength of more than 200 percent and in frequency of more than 60 percent were accomplished by varying flame-holder shape. A maximum increase in recirculation parameter of 56 percent over that for a conventional V-gutter was obtained by varying shape.

The effect of the strength and shedding frequency of the wake vortices on the combustion characteristics of flame holders is not yet known. These results may furnish the basis of correlation of combustion efficiency and stability for similarly shaped flame holders in combustion studies.

Lewis Flight Propulsion Laboratory
National Advisory Committee for Aeronautics
Cleveland, Ohio

APPENDIX A

BALSA DUST INJECTION AND SEPARATION

Balsa dust injection system. - Considerable difficulty was encountered at first in obtaining a satisfactory balsa-dust injection system. Such problems as clogging of the lines and nonuniformity of the spray pattern were eliminated by trial-and-error methods and although a number of variations were used in the early part of the investigation, the system finally adopted was found to give acceptable results at least for the range of flow conditions reported herein.

The balsa-dust chamber consisted of a cylindrical container 4 inches in diameter and 13 inches long fitted with a piston to provide a means of raising the balsa-dust level. The top of the container was made of 1-inch-thick Lucite. Air from the 125-pound service-air facility was introduced in the center of the top of the chamber through a "lawn-spray" type spinner. The service air was throttled with a small hand valve. Two diametrically opposed outlet lines were attached to the container 2 inches from the top. The balsa-dust lines (0.25-in. outside diameter thin wall copper tubing) then went to opposite sides of the calming chamber and entered the setup at a point slightly below the top screen. Spray tubes fashioned from 0.25-inch outside diameter steel tubing were installed at an angle of approximately 70° to the flow and projected through the top screen about 0.50 inch. These spray tubes were 12 inches long and were flattened in the plane of flow to provide some measure of streamlining.

Balsa-dust separator. - After several attempts were made to obtain photographic data using both balsa dust and aluminum flakes as flow tracers, the balsa dust was found to be definitely superior with respect to ease of handling and particle size (larger particles for a given weight). In addition, there was no perceptible difference between the reflectivities of the two materials.

The problem of separating chips and large particles from the usable portion of the raw sawdust was presented. Since screening the dust was found to be impractical, a centrifugal separation process was utilized. The apparatus used is shown schematically in figure 14. The essential parts of this apparatus consist of a dust container equipped with a "lawn-spray" type spinner, a settling chamber, a Lucite transition piece, and a collecting chamber. Flow was maintained through the apparatus by connecting the top of the collecting chamber to the laboratory altitude exhaust line. Room air was thus drawn through a small opening in the Lucite top of the dust container. Service air was introduced into the spinner which in turn agitated the balsa dust. The dust was then drawn through a hose line into a small annular space

formed by an aluminum bullet and the Lucite walls. The path of the flow proceeded through a narrow slot placed at 90° and to one side of the aluminum bullet (detail A). The flow path therefore had to follow a right-angle turn in a confined space and only the particles which were small enough to turn through this angle for a certain velocity in the annular space would be separated out; the remaining particles would continue on into the settling chamber. The velocity of the flow in the annular space was maintained at about 250 feet per second during the separation process.

APPENDIX B

METHOD OF DATA REDUCTION

Photographic data. - A typical flow-visualization photograph for a velocity of 19 feet per second is shown in figure 15. It will be noted that at this low velocity the individual vortex cores in the Kármán street stand out as voids in the flow field. Although these cores were not as clearly defined at the higher velocities, the photographs could be interpreted by noting that longitudinal lines drawn tangent to the sinuous path intercept at the point of tangency transverse lines drawn through the vortex centers. Lateral positions of the vortex centers were determined by taking into account voids when present, the approximate parallelism of the vortex rows, and the position of the vortices with respect to the model gutter edges.

Accordingly, for each photograph (which was enlarged to approximately 2.5 times actual size) the Kármán trail was marked with a sinuous path as shown. The wave lengths of this path represented the a spacing and the amplitudes denoted one-half the h spacing. Measurements of the a spacing were made directly from the photographs, and the arithmetic mean a spacing was determined for each flameholder model at each velocity setting.

The precision of the a spacing measurements was investigated by determining the probable error of the arithmetic mean by means of the following statistical equation:

$$r_0 = 0.6745\sqrt{\frac{v_1^2 + v_2^2 + \ldots + v_n^2}{n(n-1)}}$$

where

r_0 probable error in arithmetic mean

n number of measurements

v residual, that is, mean value minus measured value

The probable percentage error as determined from the preceding equation was of the order of 2 percent for most cases, which indicates that the method of data reduction and total number of measurements (approximately 30 for each setting) yielded sufficiently precise results. However, this equation does not account for systematic errors, which may, in turn, have affected the accuracy of the results.

Arithmetic mean values of a spacing for velocities of 25 and 50 feet per second were plotted against velocity for each flame-holder model. Although the data did not show that the a spacing was independent of velocity in all cases, the discrepancy (probably due to systematic errors) for a single flame holder as compared with the overall range of the a spacing for the various flame-holder models justified using the mean of the values for the two velocity settings. The arithmetic mean value of a spacing was therefore computed and weighted according to the number of measurements at each velocity setting.

As previously stated, the h spacing was not so well defined on the photographs as the a spacing. Because it was desirable to verify the constancy of the spacing ratio h/a for differently shaped bluff bodies two prints were chosen at random for each of several flame holders and the h spacing was determined for the downstream portion of the wake.

Velocity surveys. - The flow field downstream of the influence of the "dead water" region of the wake corresponds to the flow field obtained by superimposing a vortex field on a uniform flow field. It was reasoned (and verified by data presented in reference 4) that such a flow would yield a mean velocity curve which would be concave upward from the center line of the duct to the center line of the vortex row (assuming resultant flow is upward) because of the opposing velocity components and would be concave downward from the center line of the vortex row to some point outside the vortex band because of the additive velocity components. The h spacing could then be determined by noting the distance between the inflection point in the curve and the duct center line (h/2). A diagram of the anticipated mean velocity curve is shown in figure 16.

REFERENCES

1. Nicholson, H. M., and Field, J. P.: Some Experimental Techniques for the Investigation of the Mechanism of Flame Stabilization in the Wakes of Bluff Bodies. Bumblebee Rep. 94, Appl. Phys. Lab., Johns Hopkins Univ., Dec. 1948. (Bur. Ordnance, U.S. Navy Contract NOrd 7386.)

2. Williams, Glenn C.: Basic Studies on Flame Stabilization. Jour. Aero. Sci., vol. 16, no. 12, Dec. 1949, pp. 714-722.

3. deBothezat, George: An Introduction to the Laws of Air Resistance of Aerofoils. NACA Rep. 28, 1920.

4. Fage, A., and Johansen, F. C.: On the Flow of Air Behind an Inclined Flat Plate of Infinite Span. R. & M. 1104, British ARC, Feb. 1927.

5. Rosenhead, L., and Schwabe, M.: An Experimental Investigation of the Flow Behind Circular Cylinders in Channels of Different Breadths. Proc. Roy. Soc. (London), vol. 129, ser. A, no. 809, Sept. 3, 1930, pp. 115-135.

6. Glauert, H.: The Characteristics of a Kármán Vortex Street in a Channel of Finite Breadth. R. & M. 1151, British ARC, Dec. 1927.

7. Richardson, E. G.: Aeolian Tones. Proc. Phys. Soc. (London), vol. 36, pt. 3, April 15, 1924, pp. 153-165.

8. Kovásznay, L. S. G.: Hot-Wire Investigation of the Wake Behind Cylinders at Low Reynolds Numbers. Proc. Roy. Soc. (London), ser. A, vol. 198, no. A1053, Aug. 15, 1949, pp. 174-190.

9. Relf, E. F., and Simmons, L. F. G.: The Frequency of Eddies Generated by the Motion of Circular Cylinders through a Fluid. R. & M. 917, British ARC, June 1924.

10. Fage, A., and Johansen, F. C.: The Structure of Vortex Sheets. Phil. Mag. and Jour. Sci., ser. 7, vol. 5, Feb. 1928, pp. 417-441.

11. Ossofsky, Eli: Constant Temperature Operation of the Hot-Wire Anemometer at High Frequency. Rev. Sci. Instr., vol. 19, no. 12, Dec. 1948, pp. 881-889.

12. Rayleigh: Aeolian Tones. Phil. Mag. and Jour. Sci., ser. 6, vol. XXIX, April 1915, pp. 433-444.

TABLE I - PRINCIPAL VARIATIONS IN FLAME-HOLDER DESIGN

Flame-holder model	Method of accomplishing change in vortex strength		Description					
			Gutter details		Tabs or airfoil sections	Vortex generator details		
			Projected width, b (in.)	Gutter shape		Airfoils or flat plates	Number	Span (in.)
1	Varying velocity gradient at gutter edge	Changing gutter shape	0.75	V				
1A			1.50	V				
2			0.75	Cambered V				
2A			0.88	Cambered V				
3			0.75	Extended V				
4			0.75	U				
5		Adding edge tabs or airfoils		V	Knife edges upstream of gutter edge			
6			0.75	V	Knife edges even with gutter edge			
7			0.75	V	Rounded tabs			
8			0.75	V	Airfoils parallel with gutter edge			
9	Superimposing a vortex system on shed vortices	Mounting vortex generators on gutter	0.75	V		Airfoils	4	0.25
10			0.75	V		Flat plates	4	0.25
11			0.75	V		Flat plates	2	0.56
12		Mounting vortex generators upstream of gutter		Extended V		Flat plates	2	0.56
Cylinder			0.75					
Flat plate			0.75					

TABLE II - MEASURED VARIABLES AND CALCULATED PARAMETERS FOR APPROACH AIR-STREAM VELOCITY OF 50 FEET PER SECOND

Flame-holder model	Approach air-stream velocity V_0 (ft/sec)	Adjusted air-stream velocity V (ft/sec)	Vortex shedding frequency f (cps)	Ratio f/V (1/ft)	Number of a spacing measurements	Average a spacing (in.)	Absolute velocity of vortex system, V_3 (ft/sec)	Velocity of vortex system relative to free stream u (ft/sec)	Ratio u/V	Strength of individual vortex K (ft^2/sec)	Ratio K/V (ft)	Recirculation parameter Kf/V^2	Strouhal number fb/V	Ratio a/b
1	50	62	242	3.9	95	2.66	54	8	0.1	5	0.08	0.3	0.24	3.5
2	↓	↓	208	3.4	47	2.90	50	12	0.19	7.1	0.11	0.38	0.21	3.9
3			232	3.7	40	2.65	51	11	0.18	6.0	0.10	0.36	0.23	3.5
4			283	4.6	85	2.43	57	5	0.08	3	0.05	0.2	0.29	3.2
5			183	3.0	59	3.13	48	14	0.23	9.0	0.15	0.43	0.18	4.2
6			199	3.2	80	2.86	47	15	0.24	8.8	0.14	0.46	0.20	3.8
7			186	3.0	47	2.95	46	16	0.26	9.7	0.16	0.47	0.19	3.9
8			257	4.1	81	2.53	54	8	0.1	4	0.06	0.3	0.26	3.4
9			248	4.0	65	2.59	54	8	0.1	4	0.06	0.3	0.25	3.5
10			241	3.9	72	2.67	54	8	0.1	5	0.08	0.3	0.24	3.6
11			239	3.9	73	2.60	52	10	0.16	5.3	0.085	0.33	0.24	3.5
12			242	3.9	52	2.41	49	13	0.21	6.4	0.10	0.40	0.24	3.2
1A		80	158	2.0	26	3.93							0.25	2.6
2A		64	191	3.0	64	3.20							0.22	3.6
Cylinder		62	192	3.1	41	3.15	50	12	0.19	7.7	0.12	0.38	0.19	4.2
Flat plate		↓	172	2.8	22	3.76	54	8	0.1	6	0.1	0.3	0.17	5.0

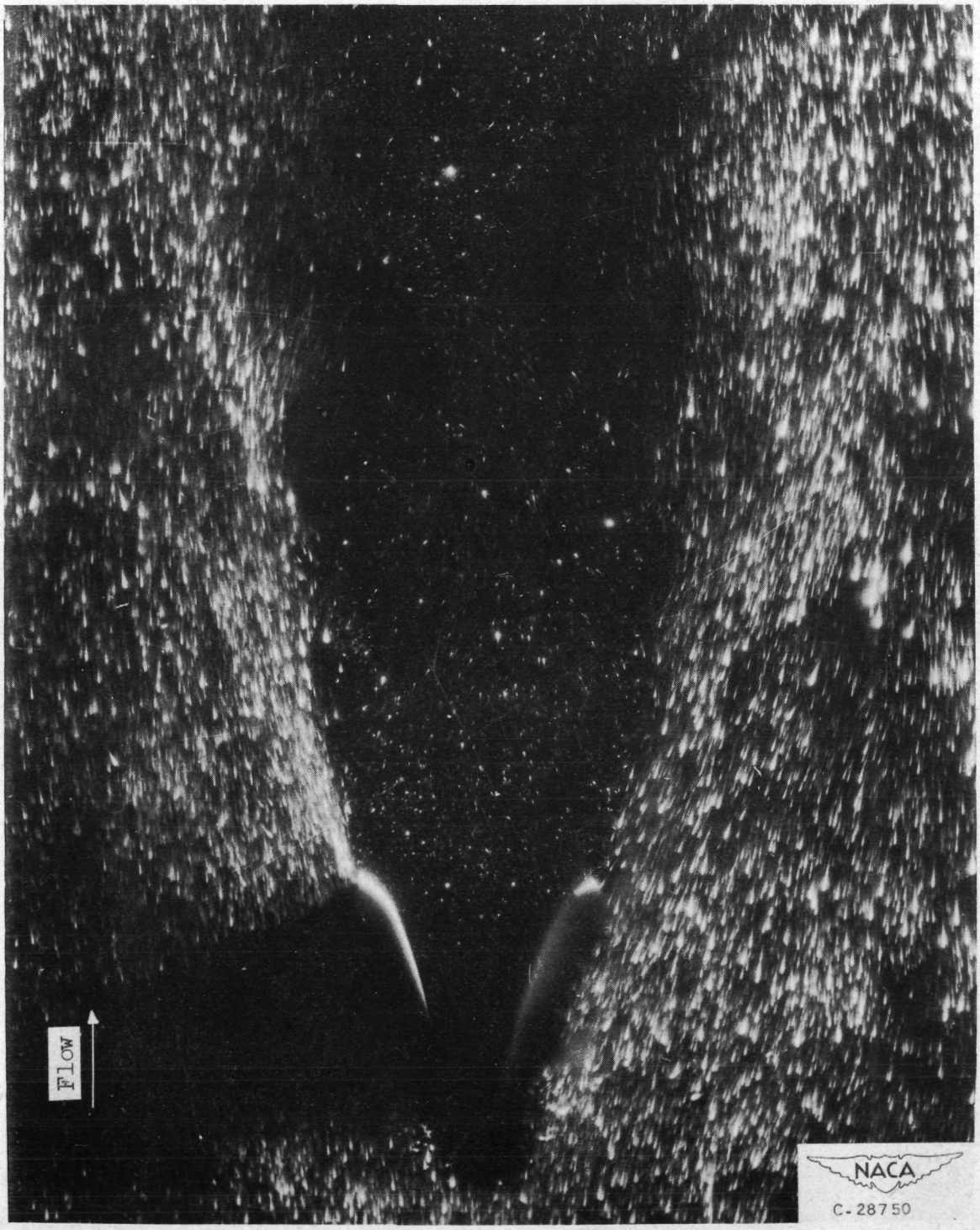

Figure 1. - Recirculation behind flame-holder model; approach air-stream velocity, approximately 50 feet per second.

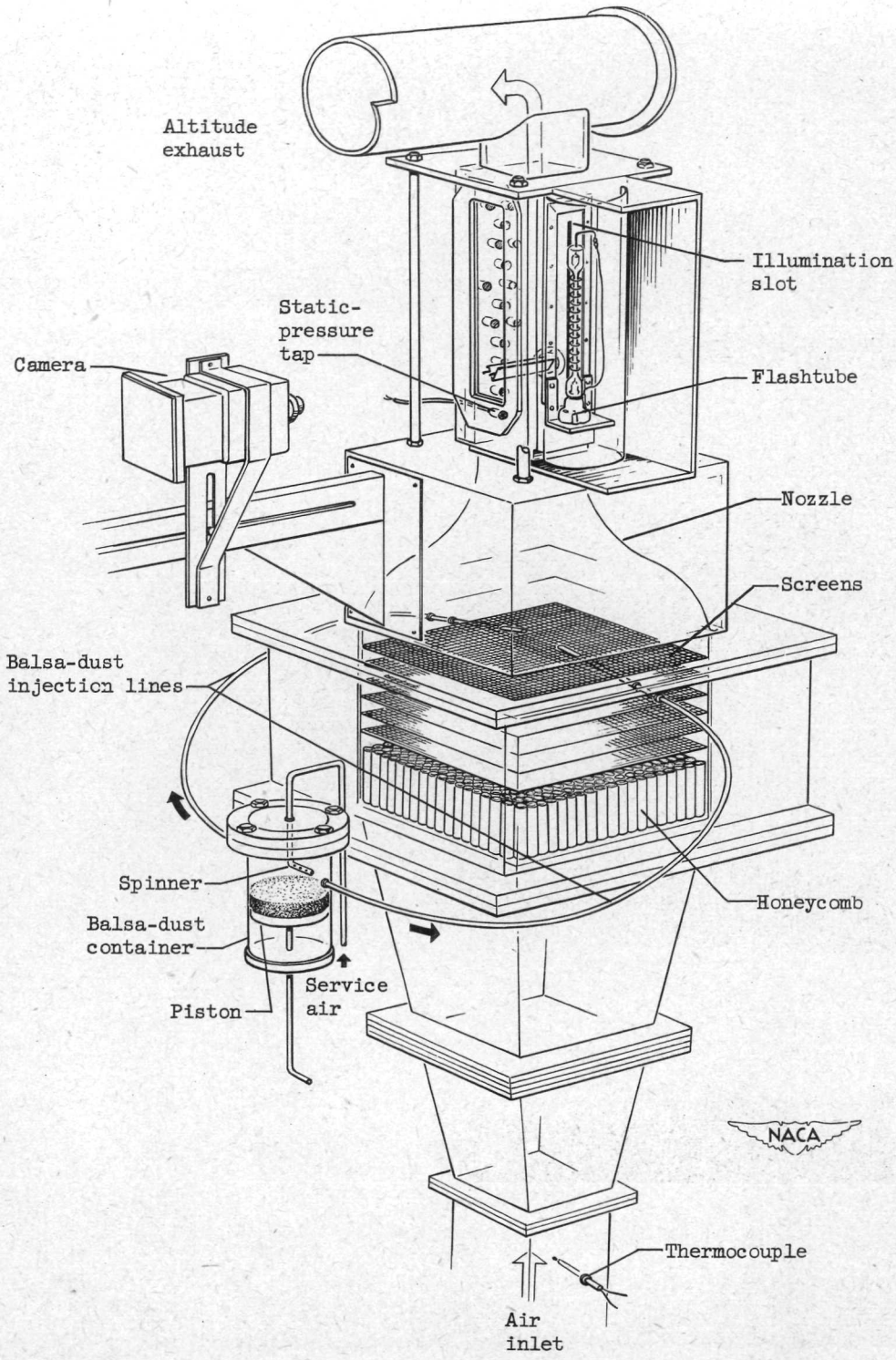

Figure 2. - Schematic diagram of flow chamber and attendant equipment.

(a) Flame holder 1. (b) Flame holder 2. (c) Flame holder 3. (d) Flame holder 4.

Figure 3. - Flame-holder models.

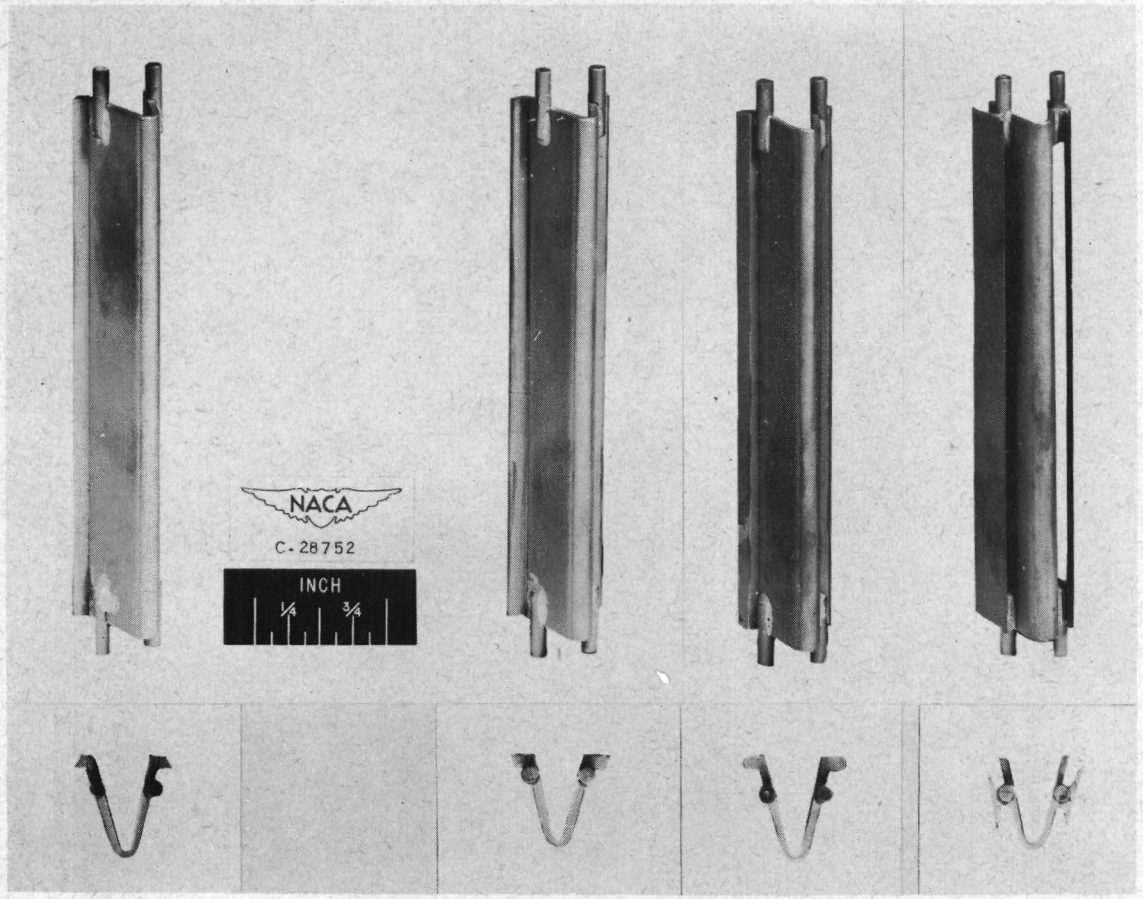

(e) Flame holder 5. (f) Flame holder 6. (g) Flame holder 7. (h) Flame holder 8.

Figure 3. - Continued. Flame-holder models.

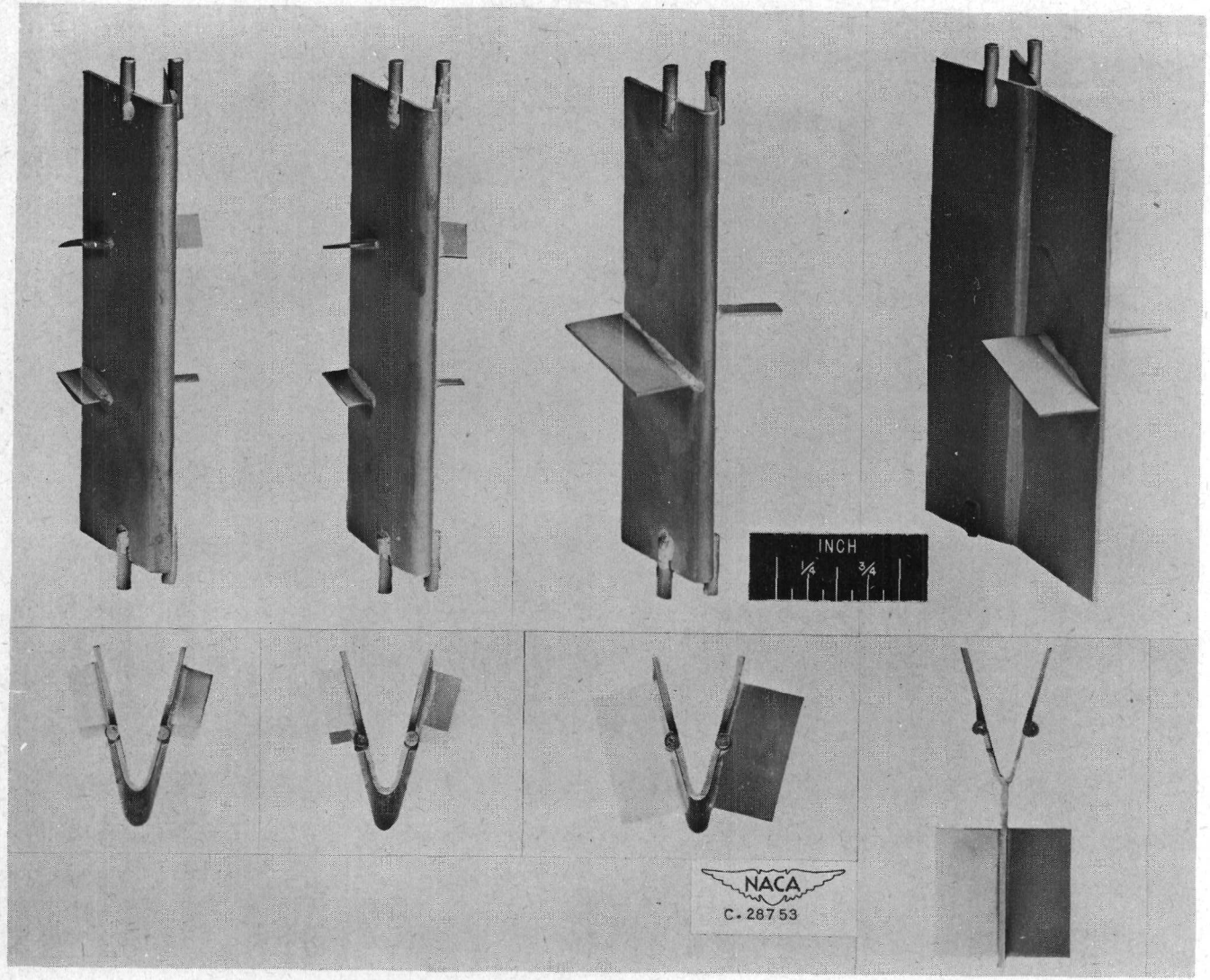

(i) Flame holder 9. (j) Flame holder 10. (k) Flame holder 11. (l) Flame holder 12.

Figure 3. - Continued. Flame-holder models.

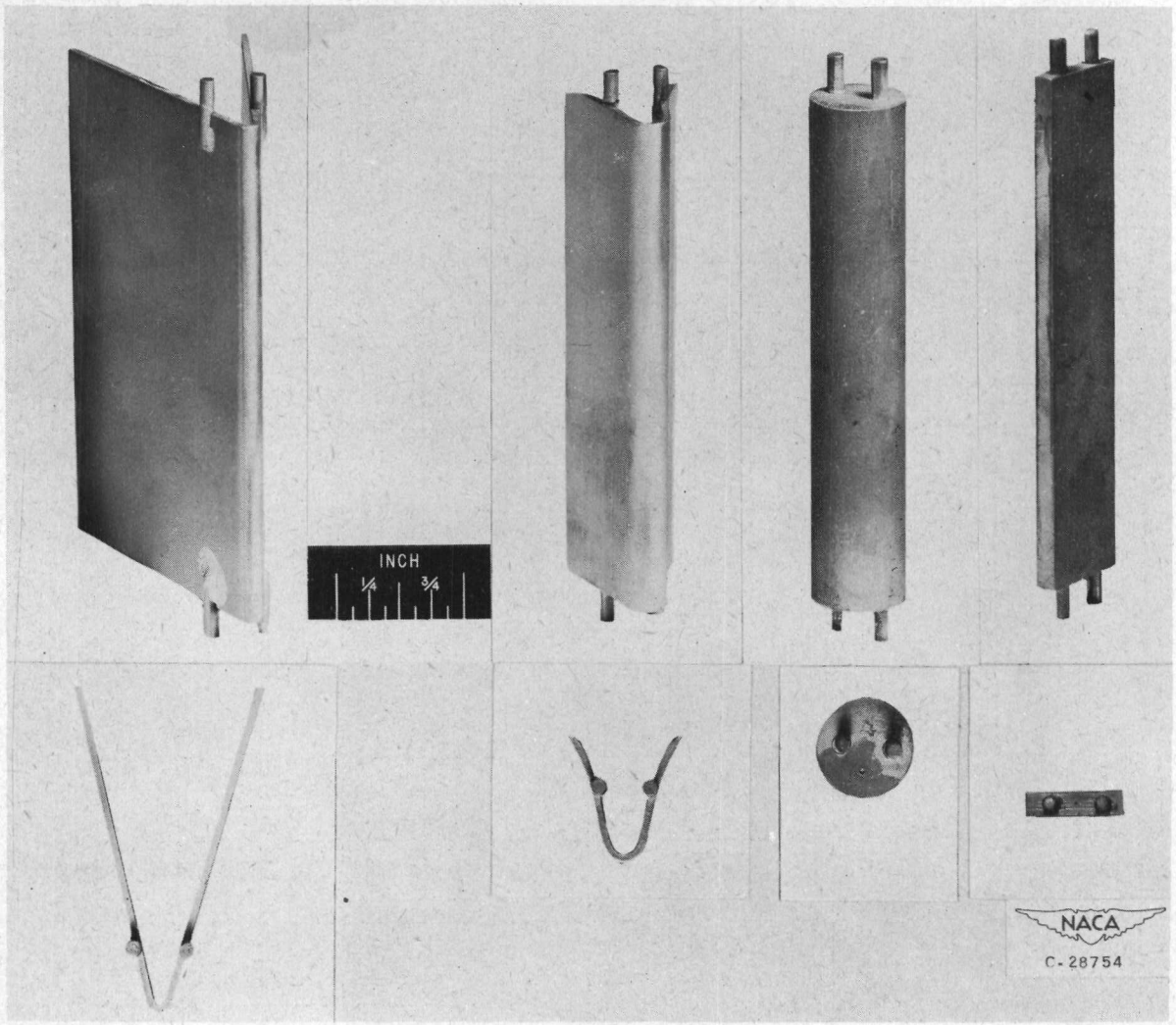

(m) Flame holder 1A. (n) Flame holder 2A. (o) Cylinder. (p) Flat plate.

Figure 3. - Concluded. Flame-holder models.

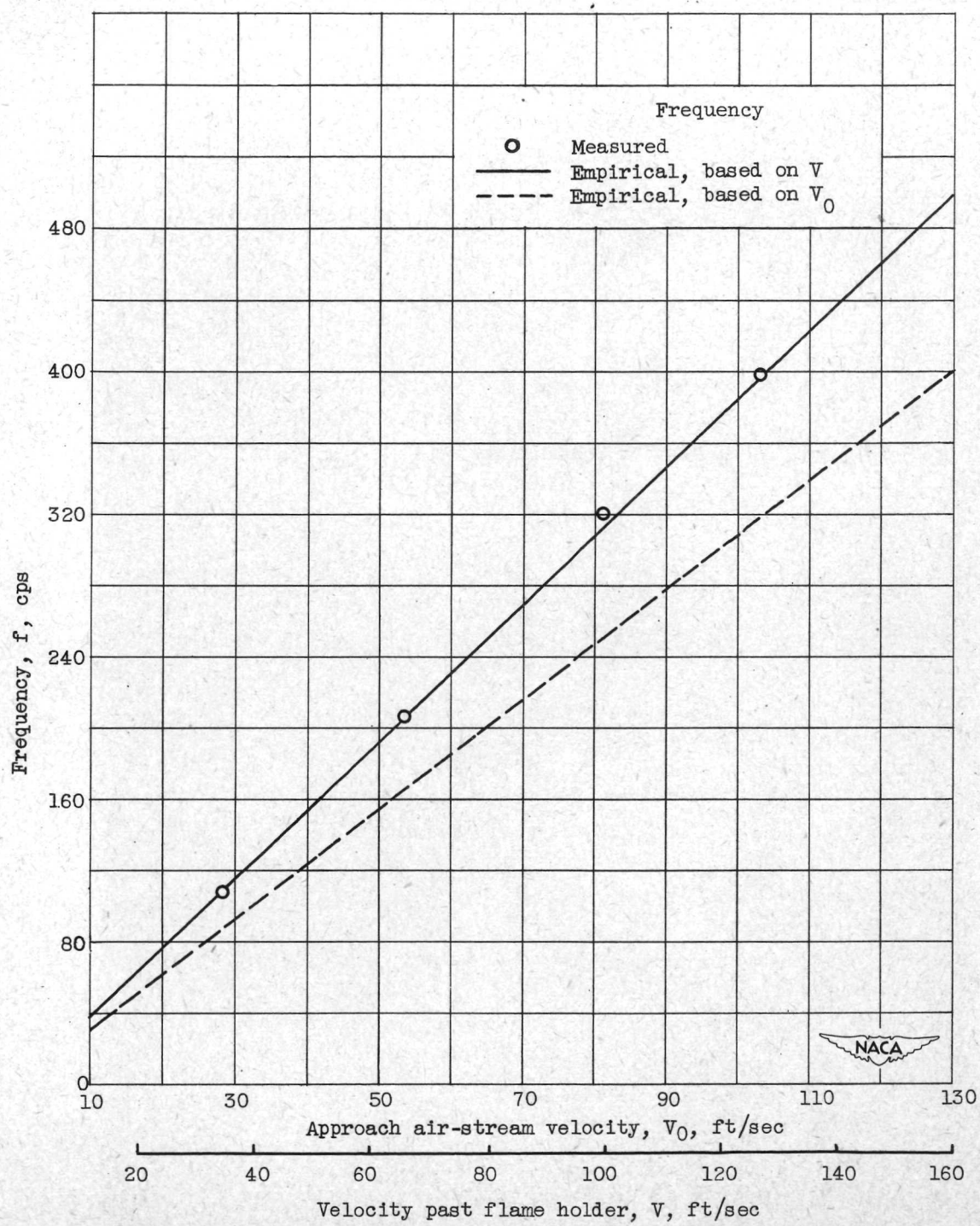

Figure 4. - Comparison of measured and theoretical frequency for circular cylinder.

Rayleigh equation: $f = \frac{0.195\ V_0}{b}\left(1 - \frac{20.1}{Re}\right)$

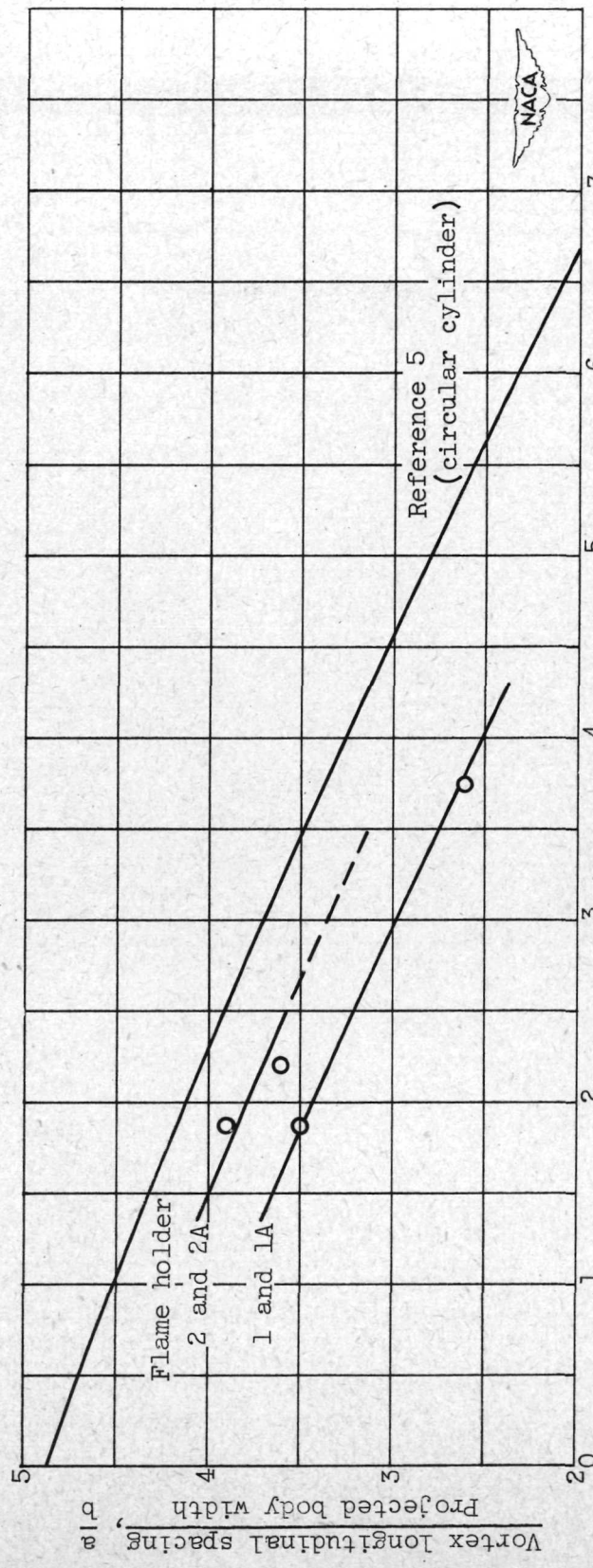

Figure 5. - Variation of ratio a/b with ratio b/H for flame holders 1, 1A, 2, and 2A, and for data from reference 5; Reynolds number greater than 400.

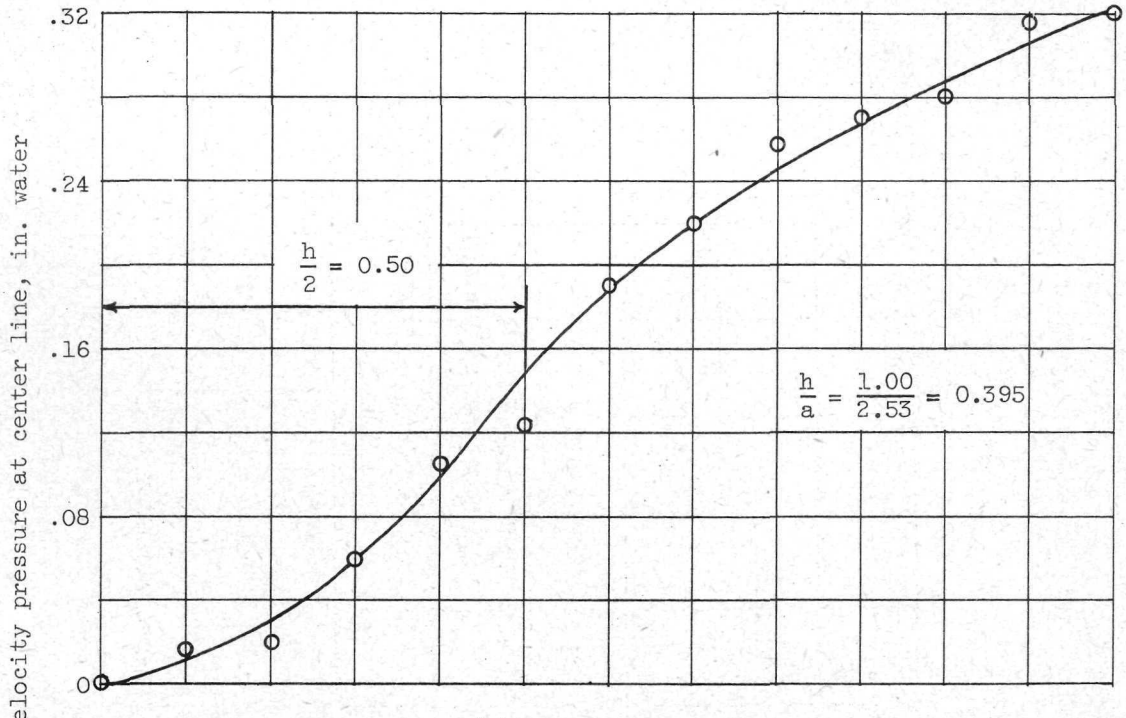

(a) Flame holder 8.

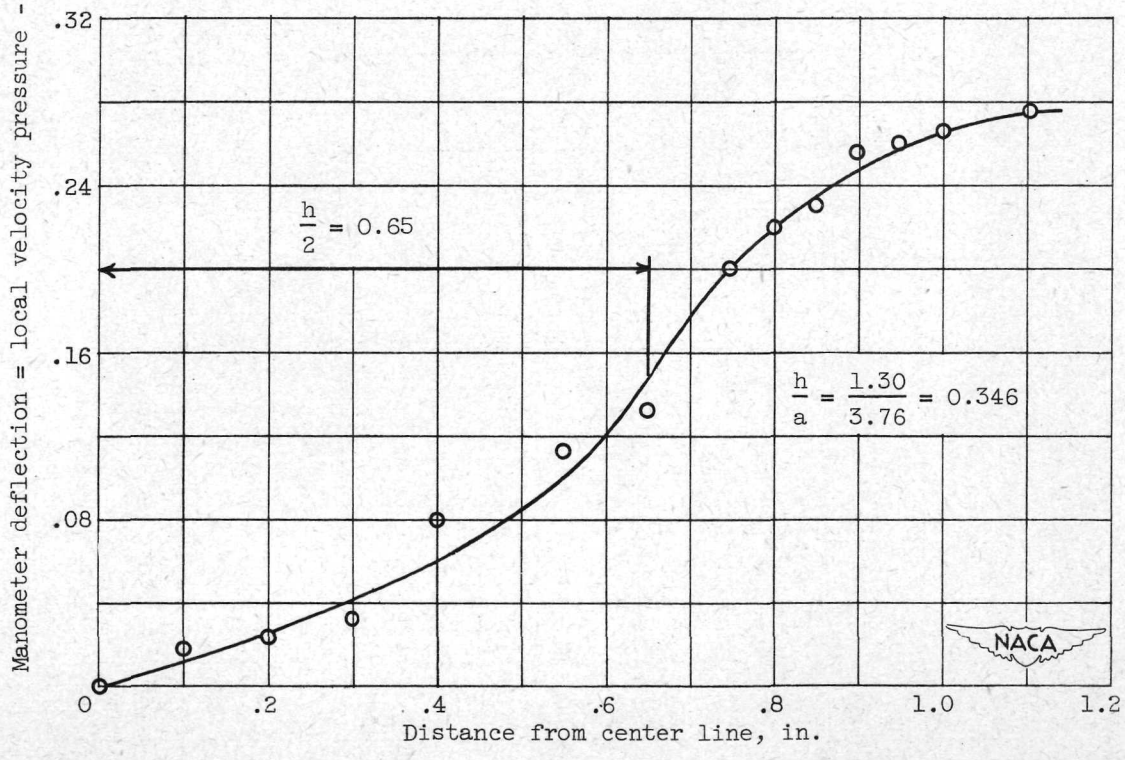

(b) Flat plate.

Figure 6. - Velocity-pressure surveys downstream of flame holders.

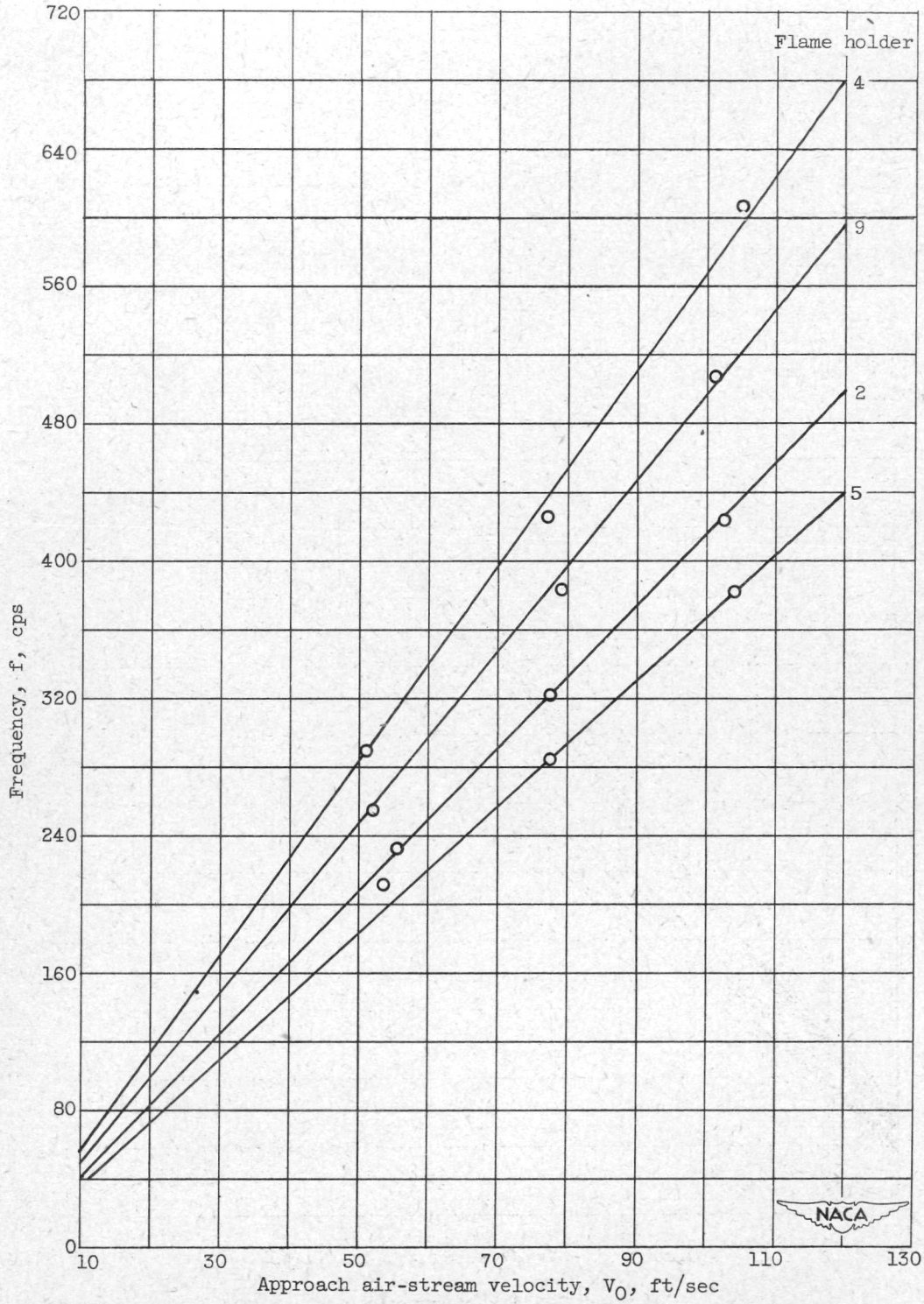

Figure 7. - Variation of vortex shedding frequency with velocity for several flame holders.

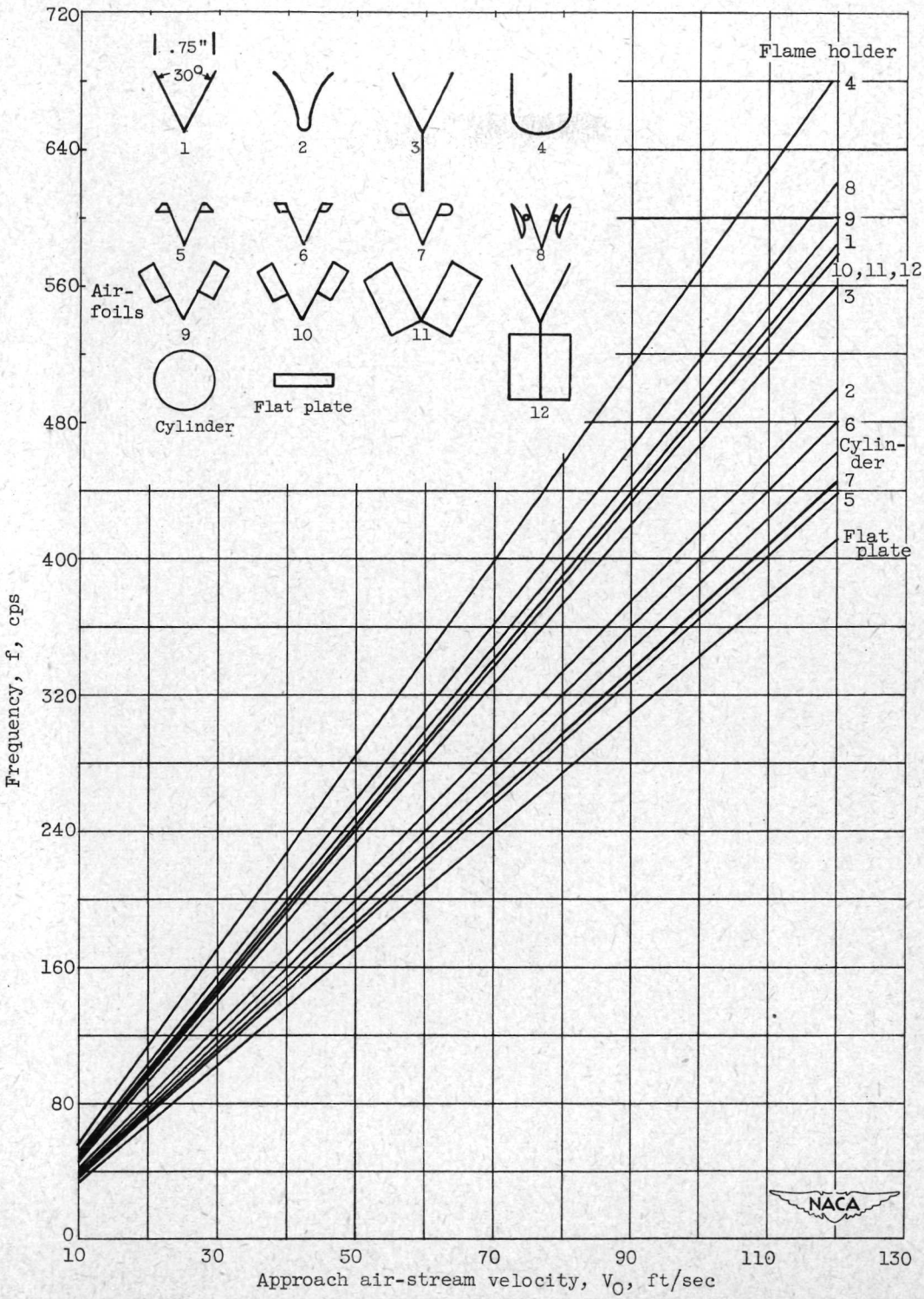

(a) Shedding frequency.

Figure 8. - Variation of shedding frequency and vortex strength with velocity for all flame holders investigated.

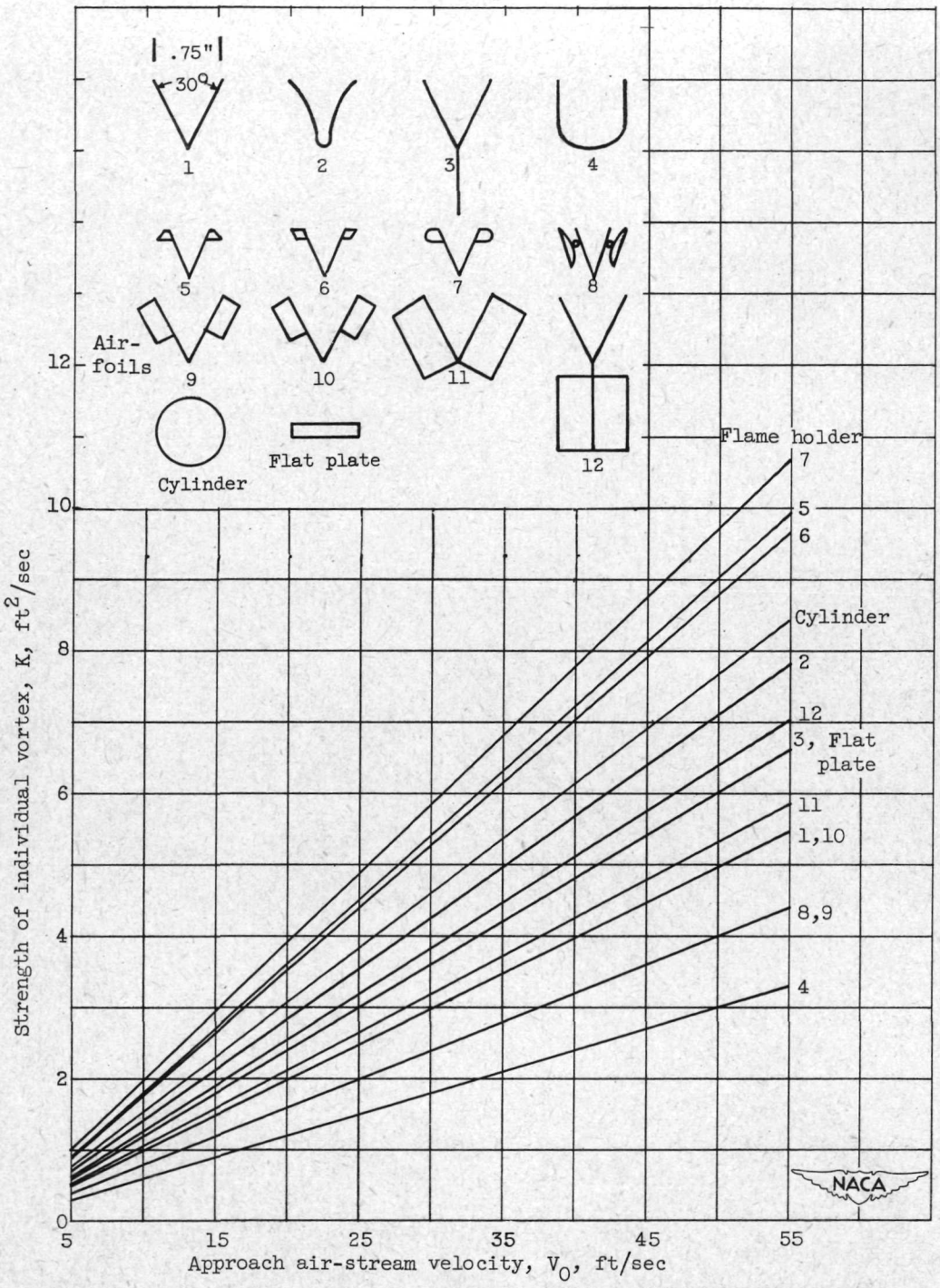

(b) Vortex strength.

Figure 8. - Concluded. Variation of shedding frequency and vortex strength with velocity for all flame holders investigated.

(a) Flame holder 4. (b) Flame holder 5. (c) Flame holder 6.

Figure 9. - Typical flow-visualization photographs at approach air-stream velocity of 25 feet per second.

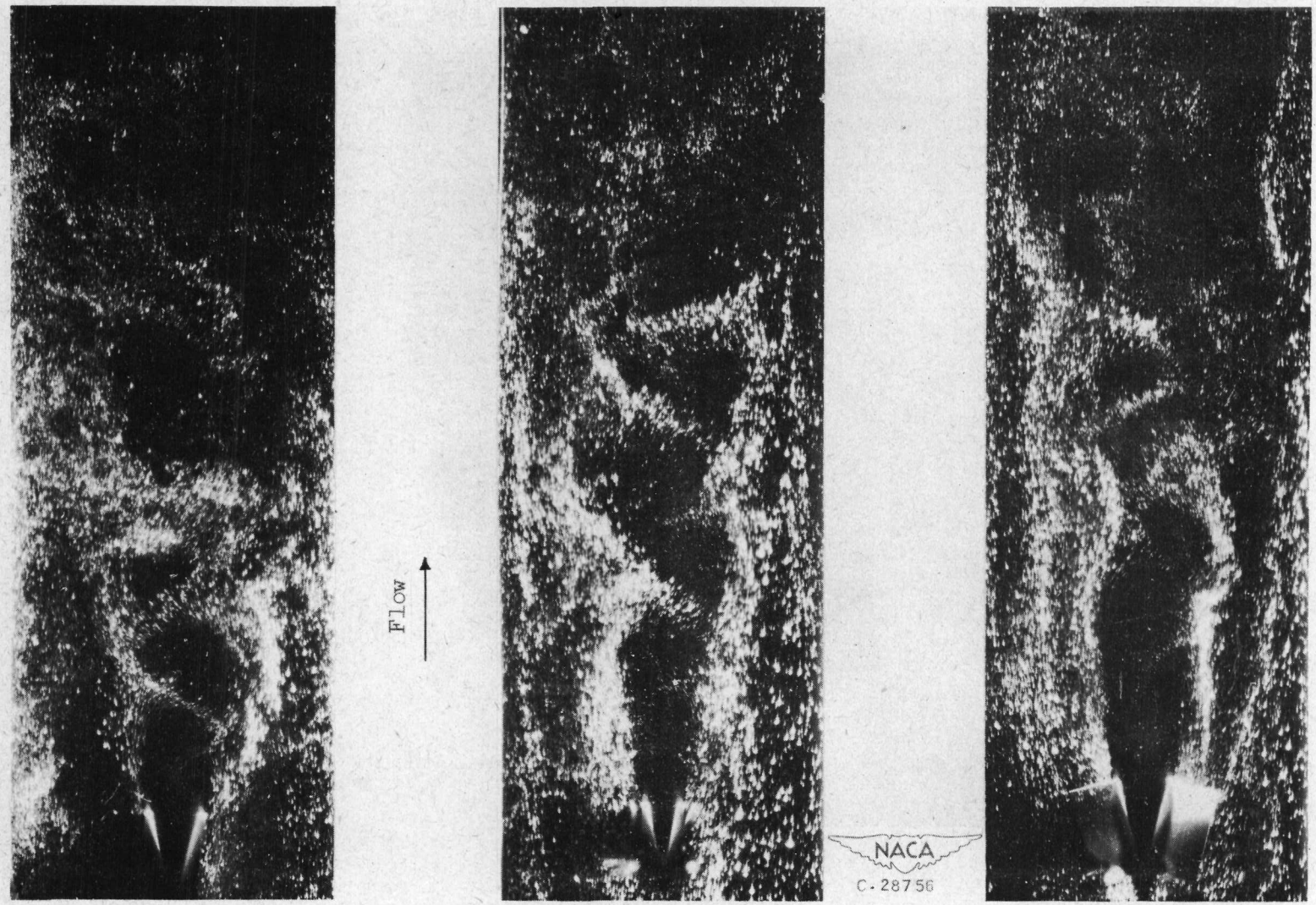

(a) Flame holder 1. (b) Flame holder 8. (c) Flame holder 11.

Figure 10. - Typical flow-visualization photographs at approach air-stream velocity of 50 feet per second.

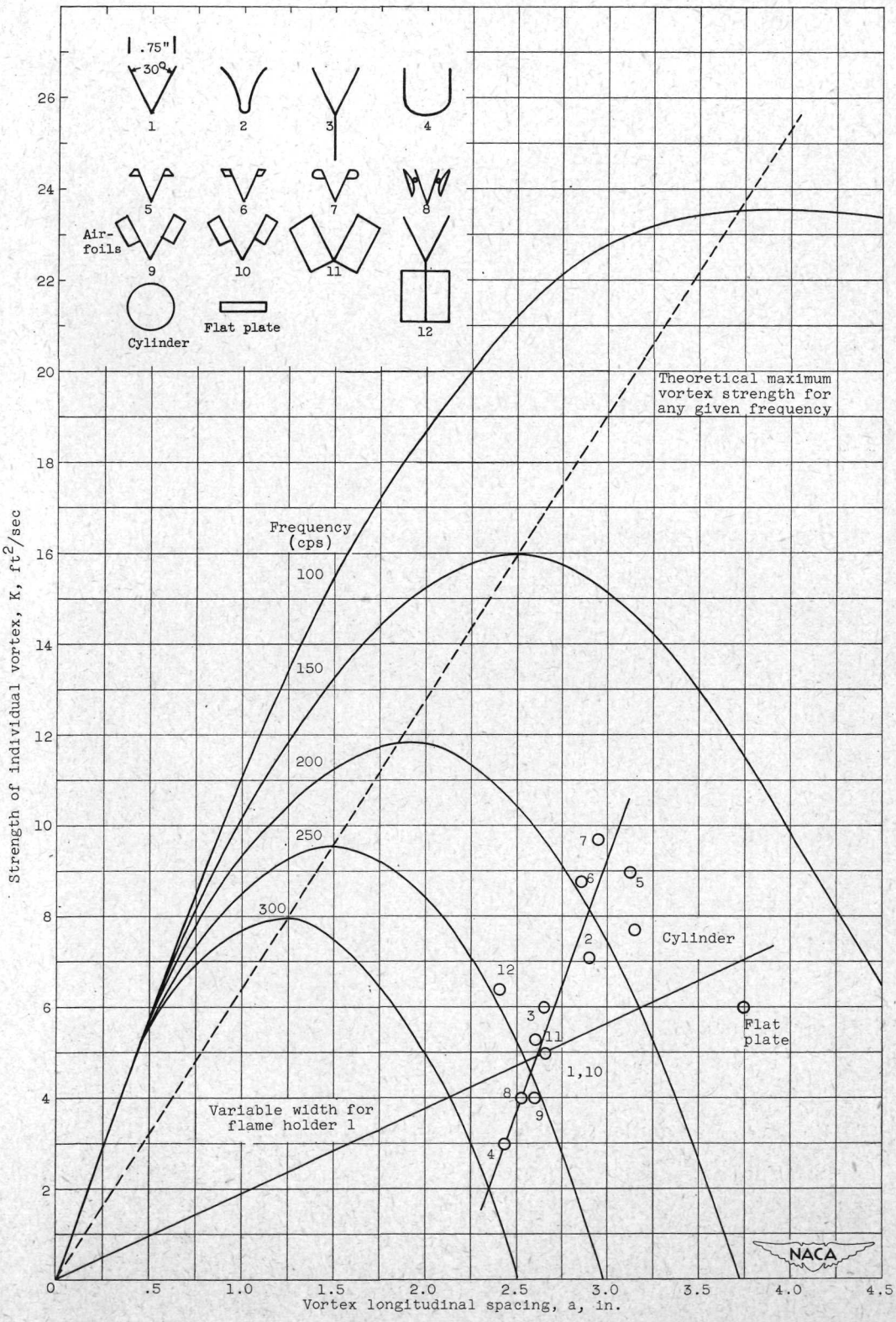

Figure 11. - Plot showing relation of experimental results to theoretical maximum vortex strength for any given frequency. Spacing ratio h/a, 0.36; air-stream velocity past flame holder, 62 feet per second.

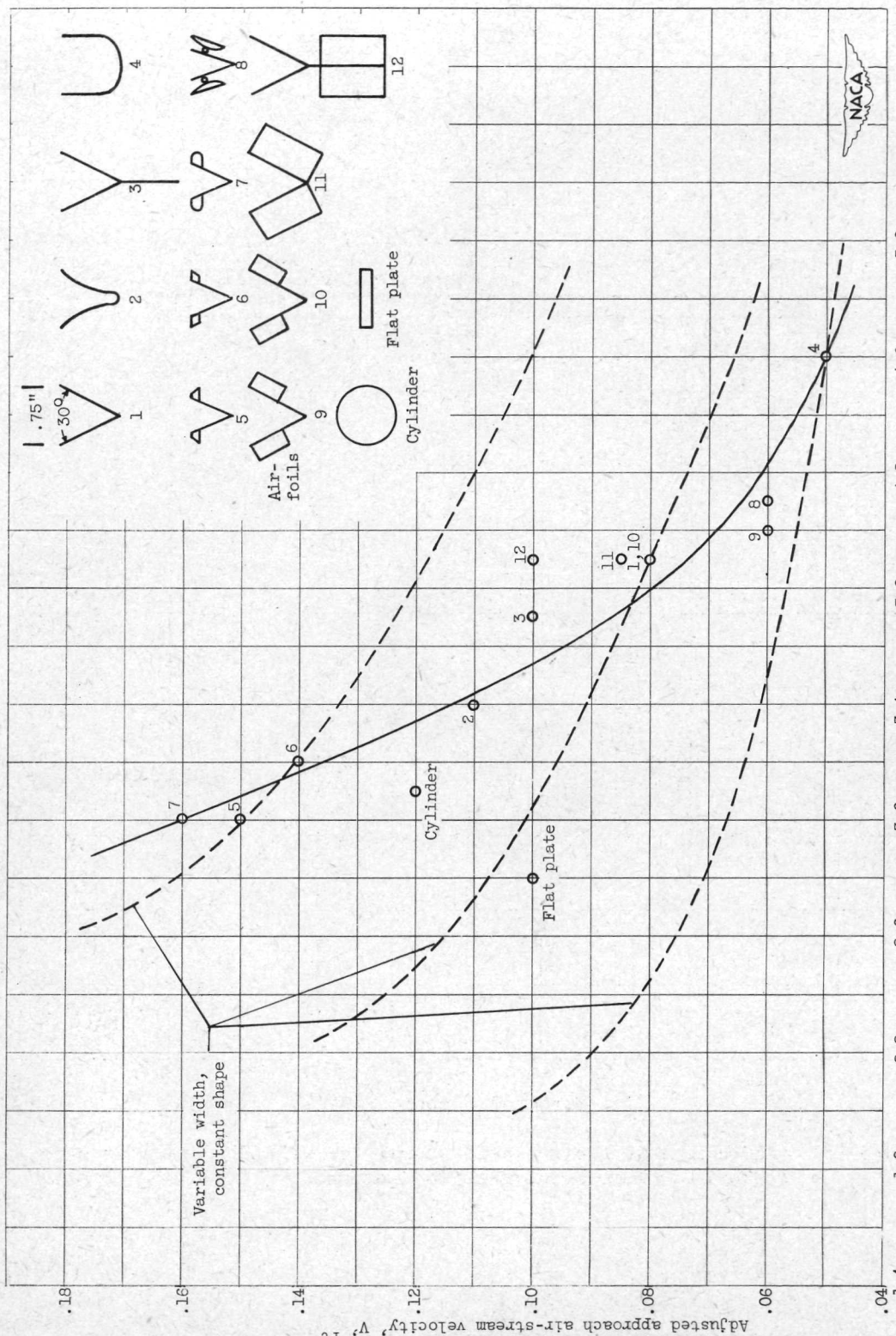

Figure 12. - Variation of K/V with f/V for all flame holders investigated.

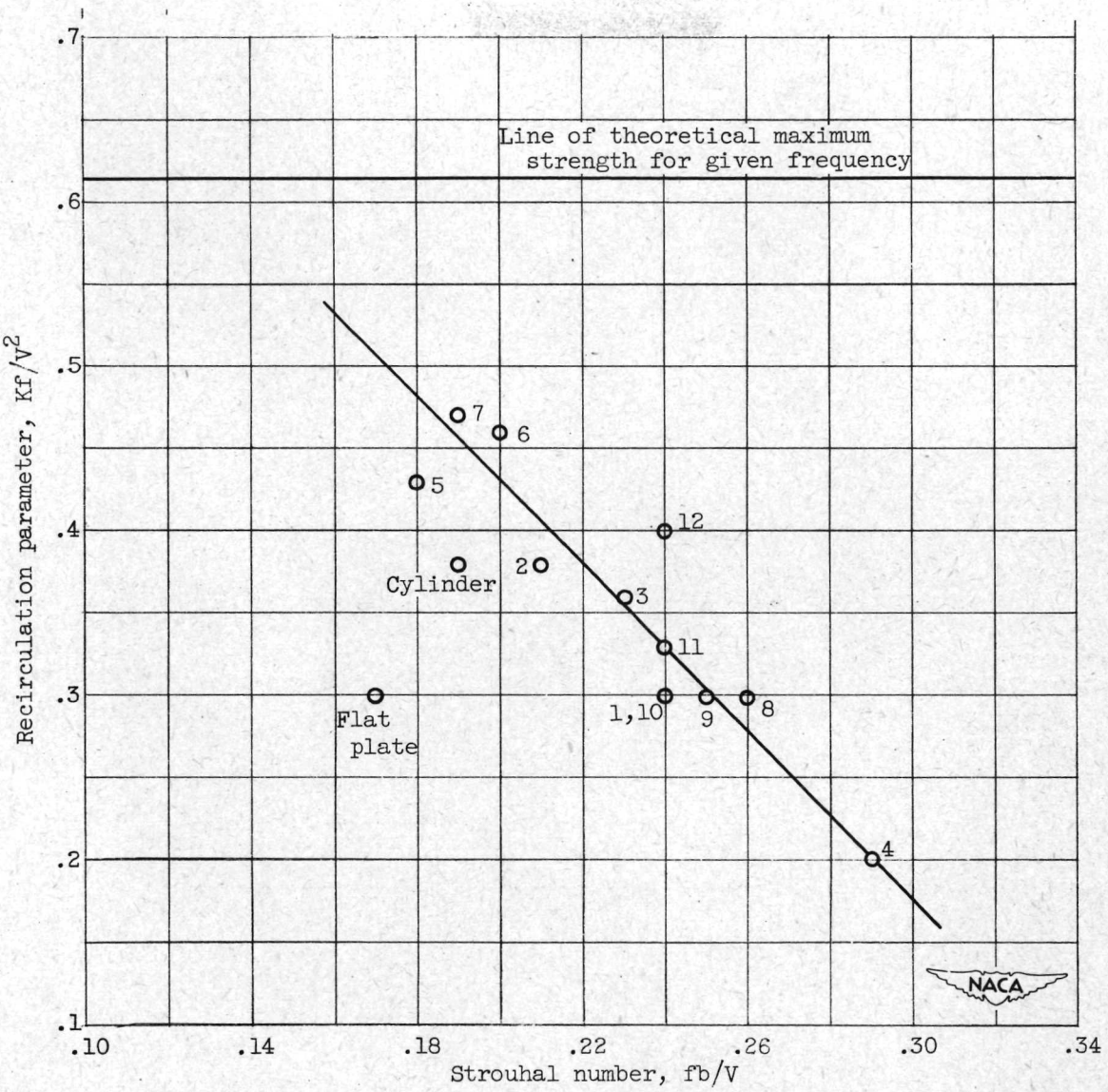

Figure 13. - Variation of recirculation parameter with Strouhal number for all flame holders investigated.

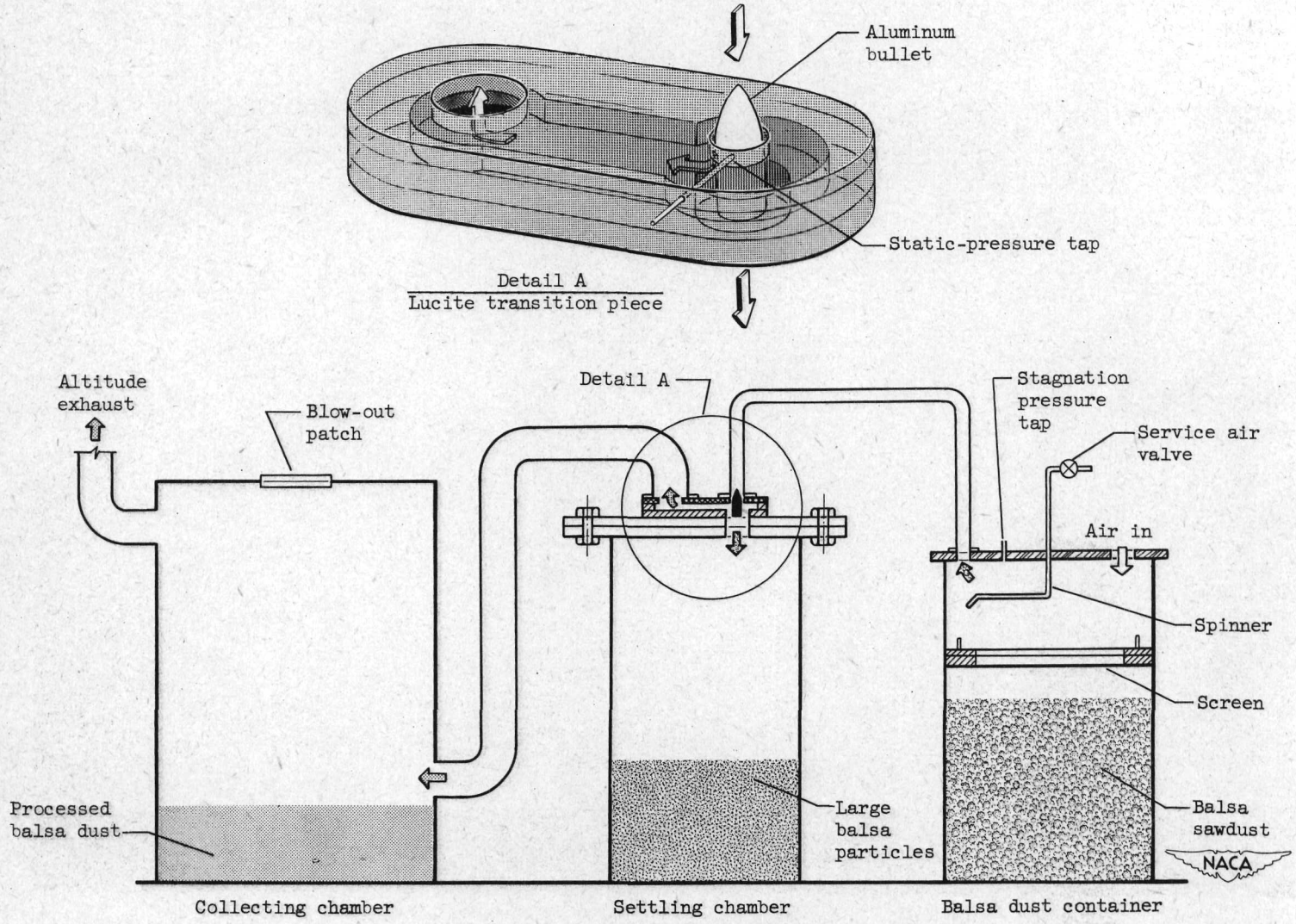

Figure 14. - Schematic diagram of balsa-dust separation apparatus.

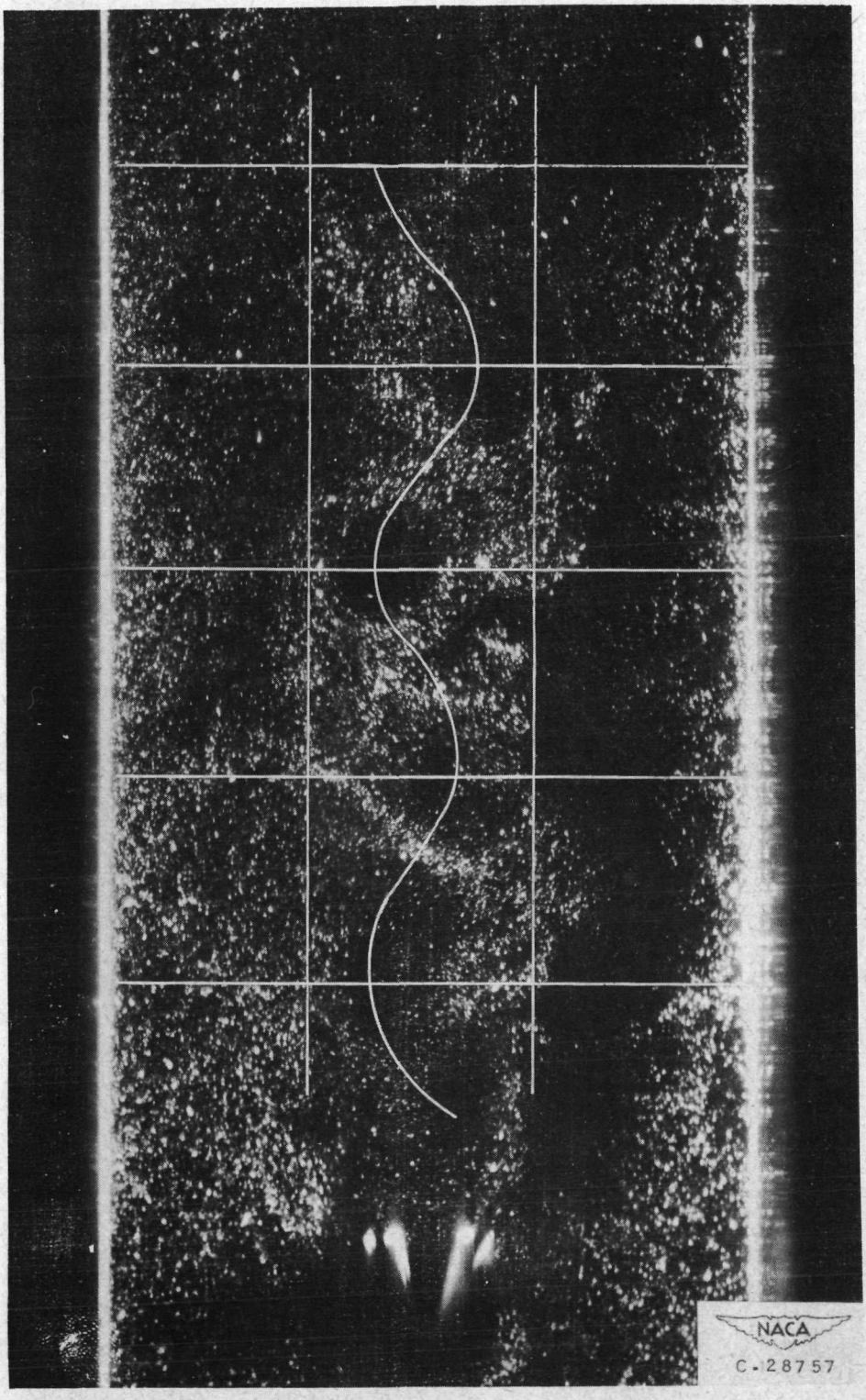

Figure 15. - Typical flow-visualization photograph showing method of marking Kármán vortex street.

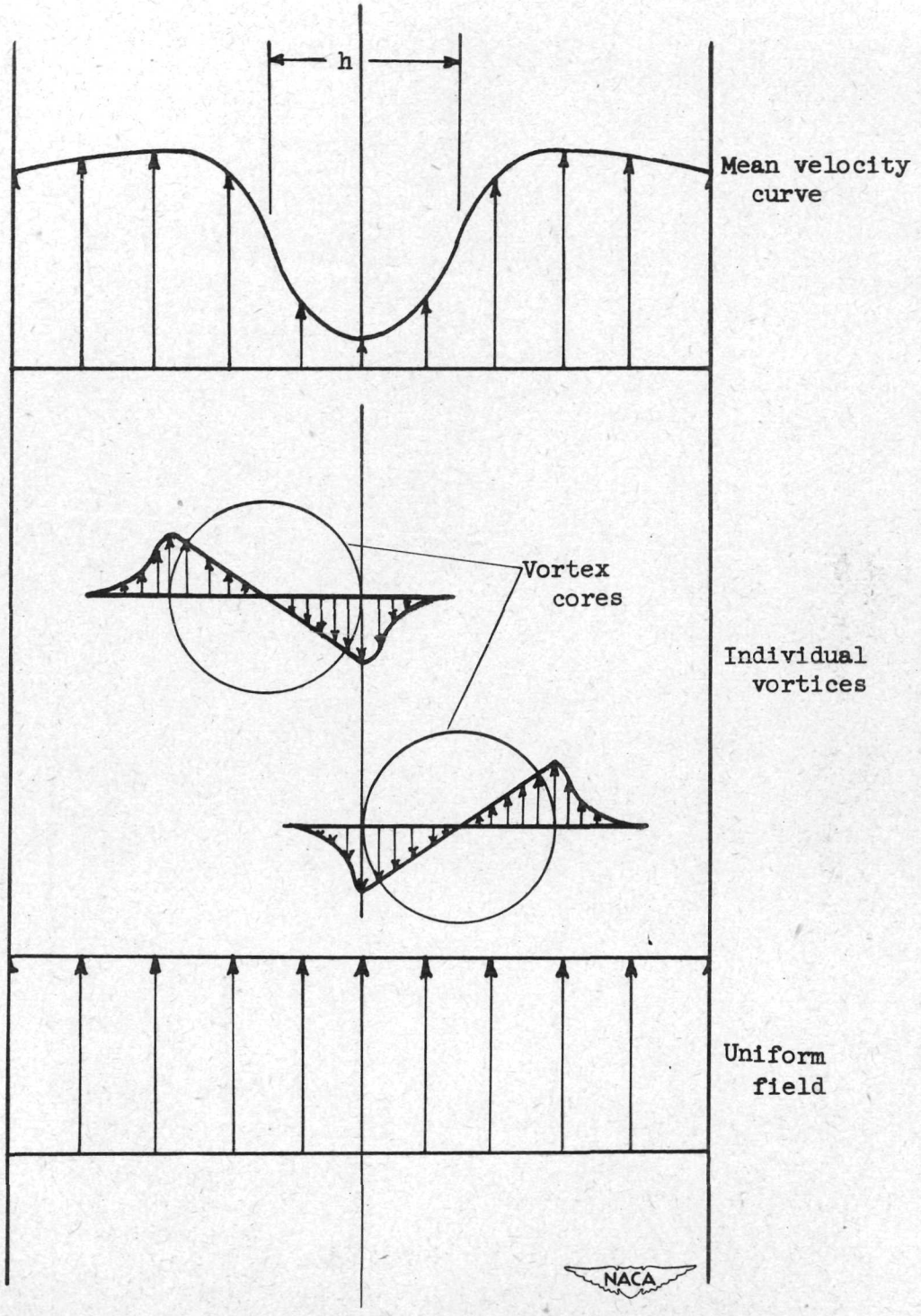

Figure 16. - Diagram showing anticipated mean velocity curve across vortex street.